BABEŞ-BOLYAI UNIVERSITY CLUJ-NAPOCA
FACULTY OF CHEMISTRY AND CHEMICAL ENGINEERING
INORGANIC CHEMISTRY SPECIALIZATION

SUMMARY OF THE PhD THESIS

ZnO-Based Electrode Materials with Tailored Properties for Supercapacitor Applications

Scientific Advisor
Prof dr. Anca Silvestru

Author
Ana Varadi

2026

Table of contents

List of Abbreviations 1

1 Introduction 3

2 Semiconductor Materials Mased on Metal Oxides: A Literature Study 6

2.1 Overview 6

2.2 Synthesis Methods of Powders Used as Electrode Materials in Supercapacitors 7

2.2.1 The Hydrothermal Method 8

2.2.2 The Precipitation Method 10

2.2.3 The Sol-Gel Method 10

2.2.4 The Microemulsion Method 12

2.2.5 Doping of ZnO Nanostructures 13

2.2.6 Decoration of Carbon Structures with Zinc Oxide 15

2.3 Characterization Methods 15

2.3.1 X-Ray Diffraction 15

2.3.2 Electron Microscopy 19

2.3.3 BET Analysis 20

2.3.4 Raman Spectroscopy 20

2.3.5 UV-Vis Spectroscopy 22

2.3.6 Photoluminiscence 22

2.3.7 Electron Paramagnetic Resonance Spectroscopy 23

2.3.8 Electrochemical Properties 24

2.4 Applications 27

3 Original Contributions 29

3.1 ZnO Nanoparticles with Different Morphologies Used as Electrode Material in SC 29

3.1.1 Introduction 29

3.1.2 Results and Discussion 30

3.1.3 Conclusions 49

3.2 Effect of Cerium Doping on the Supercapacitive Properties of ZnO Nanoflowers 50

3.2.1 Introduction 50

3.2.2 Results and Discussion 51

3.2.3 Conclusions 71

3.3 g-C_3N_4-ZnO:Cu-based Nanocomposites for Supercapacitor Applications 73

3.3.1 Introduction 73

3.3.2 Results and Discussion 74

3.3.3 Conclusions 91

4 Experimental Section 93
4.1 Equipment and Precursors 93
4.2 Synthesis of ZnO-Based Powders Used in This Study 95
4.2.1 ZnO with Nano-Rods Morphology (ZnO-NR) 95
4.2.2 ZnO with Hexagonal (ZnO-Hexa), Pyramidal (ZnO-NP) and Bullet (ZnO-NB) Morphology 96
4.2.3 ZnO with Nano-Flower Morphology (ZnO-NF) 97
4.2.4 Doping of ZnO Nanoflowers with Cerium or Copper Ions 97
4.2.5 Incorporation of ZnO:Cu onto g-C3N4 Carbon Structure 98

5 General Conclusions 100
References 102
A Apendix 128

Introduction

With technological progress, the demand for electric energy has reached unprecedented levels. This continuous increase in consumption, however, faces the limited availability of traditional energy sources. Currently, most of the electricity used in modern society comes from fossil fuels, such as oil or natural gas, resources that are unfortunately exhaustible and finite. Another disadvantage of excessive fossil fuel use is the major adverse effects on the environment. Burning coal, oil, and natural gas leads to high emissions of carbon dioxide (CO_2) and other greenhouse gases, significantly contributing to climate change. In addition, air and water pollution, loss of biodiversity, and soil degradation are direct consequences of fossil fuel extraction and use. On the other hand, there are inexhaustible and therefore infinite sources of electric energy that are still little explored and utilized. Represented by solar, wind, hydro, tidal, geothermal energy, etc., these sources have the disadvantage of being intermittent and dependent on specific weather conditions or geographic locations. Nevertheless, the only solution to meet the growing demand for electricity is to maximize the use of these inexhaustible energy sources [1].

In this context, a range of alternative energy storage technologies have been developed to be cleaner and more sustainable, thereby reducing the negative environmental impact. Among these are advanced electrochemical batteries, which include lithium-based batteries widely used in portable electronics and electric vehicles due to their high energy density and long lifespan. Emerging batteries such as lithium-sulfur [2] and lithium-oxygen [3] are also being investigated, as they can provide much higher energy densities. Additionally, batteries based on sodium, magnesium, or calcium, —more abundant and cheaper materials than lithium—are being explored, offering a less negative environmental impact [4].

Another important category is represented by supercapacitors (ultracapacitors), which store energy through electrostatic and/or redox mechanisms. They have a very high power density, fast charge-discharge rates, and extremely long lifetimes, and are often combined with batteries to create hybrid systems with high values for both energy and power density.

Faradaic or pseudo-SCs resemble conventional capacitors more than batteries. The electrodes used in this type of supercapacitor are metal oxides, predominantly

oxides of transition metals. The most commonly used are TiO_2 [16], SnO_2 [17], MnO_2 [18], RuO_2 [19], NiO [20], and ZnO [21].

The choice of electrode material is crucial for the performance of supercapacitors. Zinc oxide (ZnO) has proven to be an excellent candidate due to its remarkable properties: moderate electrical conductivity, high chemical stability, large specific surface area, and the ability to be synthesized in various nanostructured morphologies such as nanowires, nanopyramids, nanobullets, or nanorods. These structures allow easy access of ions from the electrolyte, maximizing the surface-to-volume interaction and, consequently, the specific capacity of the electrode. Moreover, ZnO exhibits biocompatibility and natural abundance, making it attractive from both sustainability and low production cost perspectives.

The electrochemical performance of ZnO can be enhanced through several strategies. Doping with metallic or non-metallic ions alters the crystal structure, defect density, and electrical conductivity of ZnO, leading to increased charge storage capacity and faster kinetics of redox reactions. Among the most studied ions are Cu^{2+}, Co^{2+}, Ni^{2+}, and Ag^{+}, which can introduce additional energy levels or facilitate electron transport [23]. Besides doping, combining ZnO with carbon-based materials such as graphene, carbon nanotubes, or carbon aerogels provides significant advantages. Carbon structures act as a conductive framework with a high specific surface area, enhancing electron transfer and stabilizing the electrode structure during repeated charge–discharge cycles. This synergy between ZnO and the carbon support can considerably increase both the energy density and cyclic stability of supercapacitors [24].

Thus, the aim of the present work is to develop ZnO-based supercapacitors with various morphologies, selectively doped and combined with carbon-based materials, representing a promising approach for obtaining energy storage devices with superior performance. Recent studies indicate that optimizing morphology, chemical composition, and interactions with the carbon support can lead to supercapacitors with energy densities comparable to batteries, but with significantly longer lifetimes and much faster charge–discharge rates, which are essential for modern applications in portable devices, electric transportation, and renewable energy storage [25].

3. Original Contributions

3.1 ZnO Nanoparticles with Different Morphologies Used as Electrode Material in SCs

The ZnO samples were synthesized using several methods: hydrothermal (for the nano-rods morphology), solvothermal (for pyramid-like, bullet, and hexagonal nanoparticles), and chemical precipitation (for the nano-flower morphology), as presented in the experimental section. These diverse morphologies were characterized using SEM and TEM microscopy.

Figure 3.1 shows the SEM-TEM images. The first sample exhibits a pyramid-shaped morphology (ZnO-NP), Figure 3.1a, with a triangular base, well-dispersed and uniform in shape. The average height of the pyramids is approximately 125 nm, with a base length of around 125 nm. Figure 3.1b shows the formation of nano-rods particles with a longitudinal morphology (ZnO-NR), having a thickness of 80 nm and lengths ranging from 500 nm to 1 m. The formation of well-defined truncated pyramid-shaped particles with a hexagonal base (ZnO-Hexa) is illustrated in Figure 3.1c, with a height of $\sim$ 150 nm and a base side length of $\sim$ 150 nm.

Another morphology is the bullet-shaped ZnO (ZnO-NB), as shown in Figure 3.1d. The height of the bullets ranges between 90 and 160 nm, with base diameters of 57 and 30 nm, respectively. Nanoparticles with a nanoflower morphology (ZnO-NF) are shown in Figure 3.1e and are formed by the agglomeration of several oval-shaped particles, with lengths ranging from 150 to 300 nm.

The Raman spectra of ZnO samples with different morphologies exhibit three peaks, as shown in Figure 3.6: E_2 (low) at 100 cm^{-1}, A_1 (TO) at 332 cm^{-1}, and E_2 (high) at 438 cm^{-1}. An additional peak at 130 cm^{-1} is also observed, corresponding to the asymmetric tail of the E_2 (low) vibration mode [137]. The E_2 (low) vibration mode has been attributed to Zn vibrations, while the A_1 (TO) mode has been associated with Zn interstitials [138].

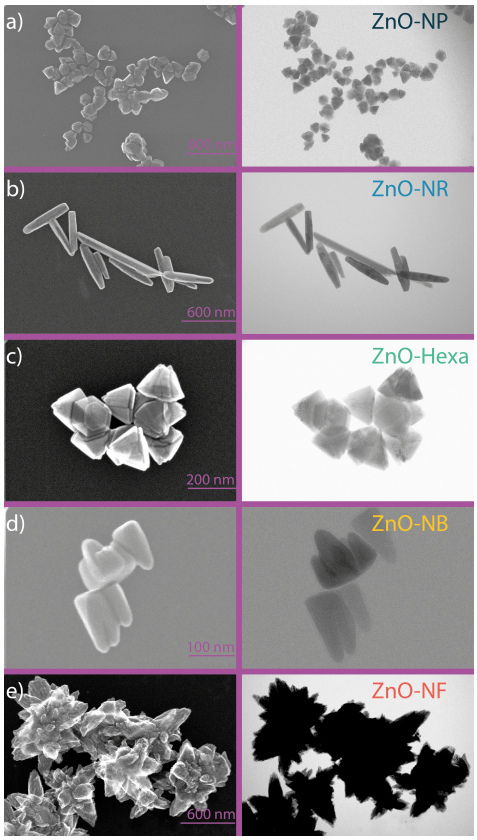

Figure 3.1: STEM images of ZnO samples with different morphologies: a) nano-pyramid (ZnO-NP); b) nano-rod (ZnO-NR); c) hexagonal (ZnO-Hexa); d) nano-bullet (ZnO-NB); e) nano-flower (ZnO-NF)

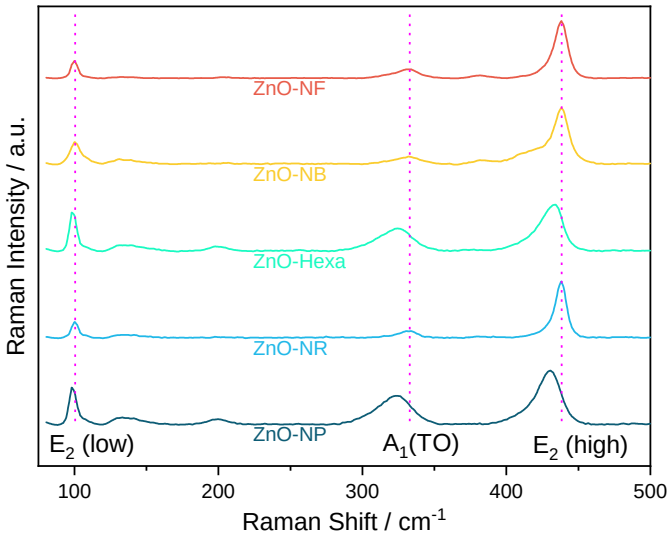

Figure 3.6: Raman spectra of ZnO samples with different morphologies

The crystalline nature of the samples was evaluated by deconvoluting the Raman spectrum using a Lorentzian function. The parameters derived from this deconvolution, particularly the Full Width at Half Maximum (FWHM) values (Table 3.2), indicate the crystallinity of the samples. Low FWHM values correspond to highly

crystalline structures. As shown in Table 3.2, ZnO-Hexa and ZnO-NP exhibit the highest FWHM values, indicating more disordered states. These results are partially consistent with the crystallite size assessments obtained from XRD. The discrepancy could be due to the limited spatial coverage of Raman measurements compared to bulk characterization techniques.

Table 3.2: The band parameters obtained from the deconvolution of the peak at 438 cm^{-1}

Sample	Intensity / u.a.	FHWM / cm^{-1}	Area / a.u.
ZnO-NR	0.93	11.13	16.25
ZnO-NB	0.96	7.96	11.95
ZnO-NF	0.99	9.39	14.55
ZnO-NP	0.85	16.29	21.86
ZnO-Hexa	0.76	12.85	15.41

The results of EPR measurements performed on ZnO particles with different morphologies are presented in Figure 3.8. All samples exhibit two distinct EPR signals, consistent with results reported in previous studies [151],[152]. The first signal, with g $\sim$ 2.005, located at low fields (320.07 mT), shows minor variations across all morphologies, while the second signal, with g $\sim$ 1.96, appearing at approximately 360 mT, shows changes in both intensity and position (g-value).

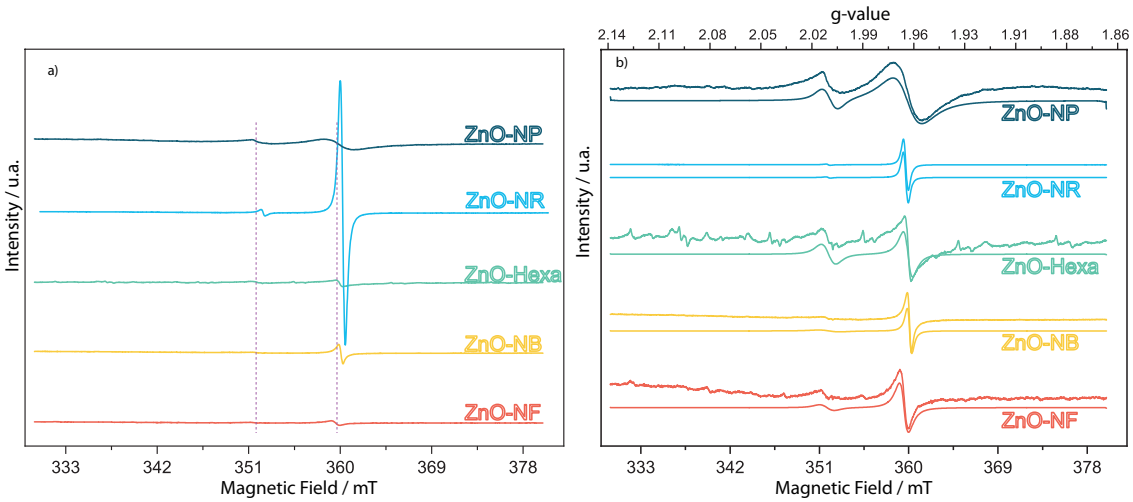

Figure 3.8: The EPR spectrum, in the X-band, of ZnO samples with different morphologies. The vertical lines indicate the positions of the "core-shell" defect centers: a) Simulation of the EPR spectrum of ZnO samples with different morphologies after normalization to the maximum intensity; b) The upper line represents the normalized EPR spectrum for each sample, while the lower line represents the simulated spectrum

CV analysis, applied to investigate the electrochemical properties of the superca-

pacitors, allowed for identifying the charge storage mechanism, evaluating the capacitive behavior, and analyzing the kinetics of the electrochemical processes [156], [157]. Figure 3.9 shows the CV curves of the supercapacitors measured at scan rates of 1, 3, 5, 7, and 10 mV/s over a potential window from 0 to 1 V. According to Figure 3.9, the current values obtained are similar for all supercapacitors and increase with the scan rate. This demonstrates that all ZnO-based materials used in the study exhibit high electrochemical stability.

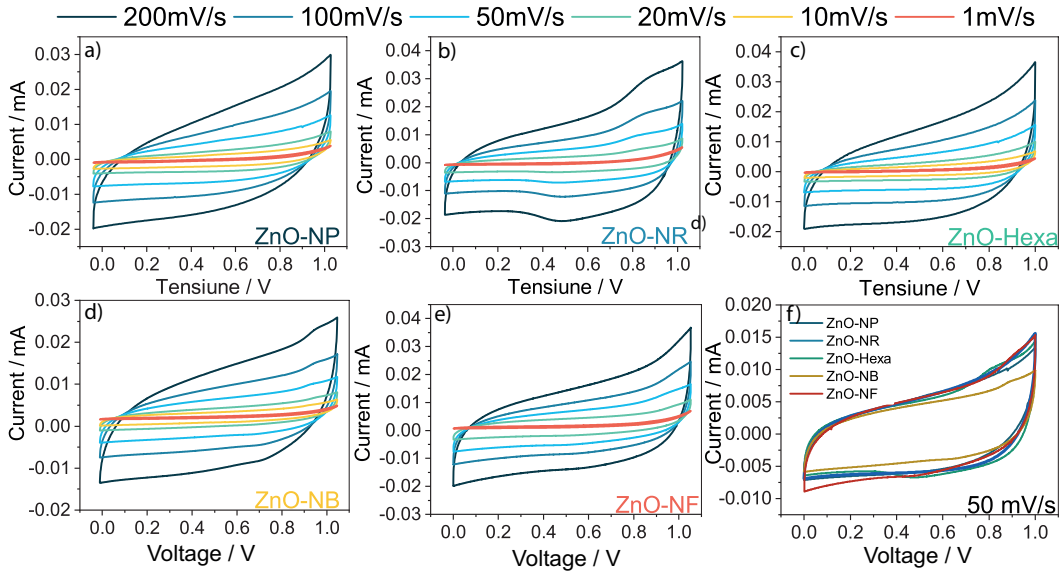

Figure 3.9: Cyclic voltammetry (CV) profiles of ZnO-based supercapacitors: (a) ZnO-NP; (b) ZnO-NR; (c) ZnO-Hexa; (d) ZnO-NB; (e) ZnO-NF and (f) CV graphs for all SCs at 50 mV/s

The specific capacitance (C_S) values of ZnO-based supercapacitors with different morphologies were calculated at various scan rates by integrating the area under the CV curve [163], as shown in Figure 3.10. The scan rate affects the kinetics of the electrochemical reaction, the double-layer capacitance, and diffusion processes [164],[165],[166]. Ionic diffusion and electrochemical reactions are more efficient at lower scan rates, which promotes a more uniform distribution of charge within the electrode and enhances ion diffusion at the surface, thereby increasing C_S by increasing the amount of active material available for ion interaction. C_S can be further improved by controlling the charge–discharge processes at the electrode surface [167].

Figure 3.10 shows that the C_S values increase significantly as the scan rates decrease from 200 to 1 mV/s. ZnO-NR-based supercapacitors exhibit the highest C_S at the slowest scan rate, approximately 181 F/g, followed by ZnO-Hexa with around 140 F/g (see Table 3.6).

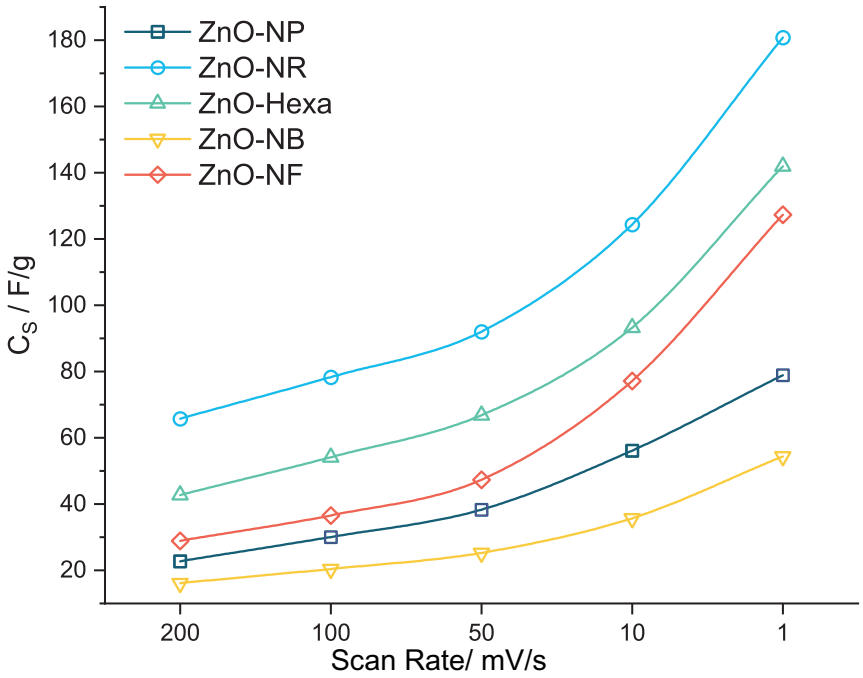

Figure 3.10: C_S values of ZnO-based SCs as a function of scan rate

Tabel 3.6: Values of specific capacitance (C_S), energy density (E_D), and power density (P_D) for the five ZnO-based electrode materials tested in SCs

Sample	C_S / F/g	E_D / Wh/kg	P_D / kW/kg
ZnO-NP	78.86	11	150
ZnO-NR	180.78	25	211
ZnO-Hexa	141.93	19	252
ZnO-NB	54.35	7	158
ZnO-NF	127.33	17	163

Figure 3.12a shows the time–voltage curves of ZnO-based SCs with different morphologies used as electrode materials. In the GCPL analysis, the 'time vs. voltage' plot represents the temporal evolution of the electrode potential [168]. The curves illustrate how the electrode potential changes during the charging and discharging processes, showing similar behavior for all SCs, which suggests that the electrode material morphology does not significantly affect the charge/discharge process. Long charge/discharge durations indicate the electrode's ability to store and release energy. This may imply favorable electrode characteristics, such as high capacitance and low internal resistance.

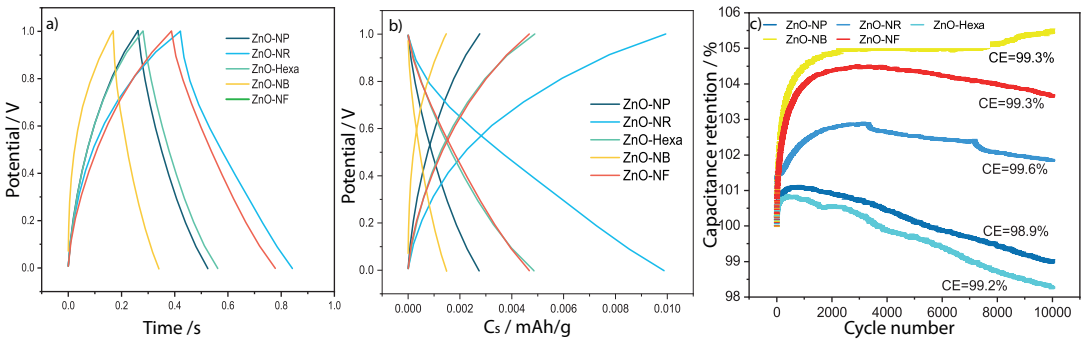

Figure 3.12: a) Time versus voltage; b) Specific capacitance versus voltage; c) Capacitance retention for ZnO-based SCs with different morphologies.

ZnO-NR nanoparticles exhibited the highest specific capacitance value, approximately 181 F/g. The energy and power densities of ZnO-NR were 25 Wh/kg and 211 kW/kg, respectively. Consequently, modifying the surface morphology of the material leads to changes in the crystal structure and its quality, specific surface area, paramagnetic defects, band gap energy, and electrochemical properties. Compared to other ZnO-based materials with different morphologies reported in the literature, ZnO-NR stands out for its electrical properties. Moreover, a capacitance retention value of approximately 100% after 10,000 cycles indicates exceptional electrochemical performance, making them ideal for applications requiring high power density, such as high-performance computing centers, electric vehicle charging stations, and space technology.

3.1.3 Conclusions

- Modification of the surface morphology of ZnO-based materials leads to changes in crystal structure, specific surface area, type of paramagnetic defects, band gap energy, and electrochemical properties.
- Compared to other ZnO morphologies reported in the literature, ZnO-NR exhibits superior electrical properties.
- The analyzed materials demonstrated high electrochemical stability, with ZnO-NR showing a capacitance retention of 100% after 10,000 cycles.
- ZnO nanoparticles with elongated, hexagonal, and nanoflower morphologies exhibited high electrochemical performance, with specific capacitance values of 180, 142, and 127 F/g, respectively.

- The ratio between zinc and oxygen vacancies represents a key factor in determining the energy storage performance of ZnO-based materials.
- The ZnO-NR sample exhibited the highest EPR signal intensity and the highest ratio between internal and external defect centers.
- ZnO-NR and ZnO-NF samples showed the narrowest band gap, leading to improved conductivity and enhanced electron and ion mobility, thereby reducing energy consumption.
- The obtained results indicate the potential of these materials for applications requiring high power density, such as high-performance computing centers, electric vehicle charging stations, and space applications.

3.2 Effect of Cerium Doping on the Supercapacitive Properties of ZnO Nano- flowers

As expected for mesoporous materials, both undoped and Ce-doped ZnO samples exhibit typical type IV N_2 adsorption isotherms, shown in Figure 3.16 along with the pore size distribution. The specific surface areas (S_{BET}) of Ce-doped ZnO samples show a slight increase compared to the undoped sample (see Table 3.8). Thus, while undoped ZnO has a S_{BET} of only 6.9 m^2/g, Ce doping leads to a maximum value for ZnO:Ce0.4, with S_{BET} = 13.8 m^2/g. The S_{BET} values decrease with increasing dopant concentration, a trend also observed in the pore size distribution. Although minor changes are observed in both S_{BET} and pore distribution, the morphology and structure of ZnO nanoflowers are not significantly affected by Ce ion doping.

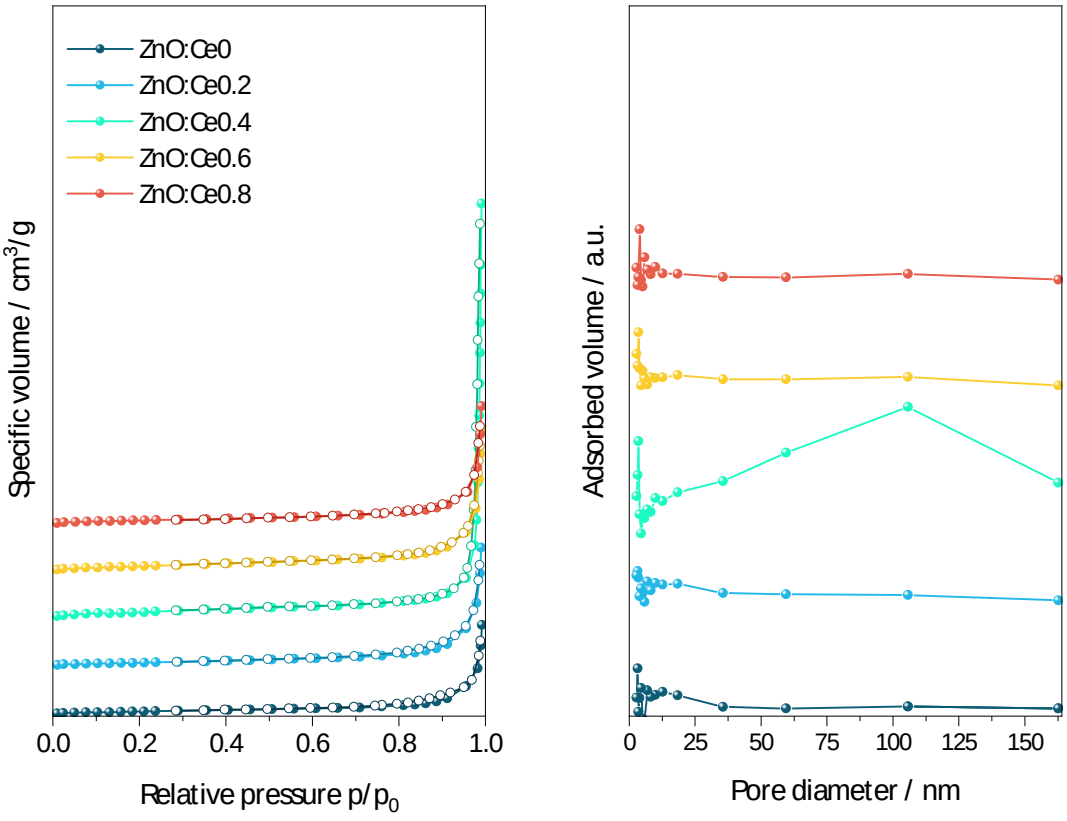

Figure 3.16: N_2 adsorption isotherms and pore size distribution of ZnO:Ce samples.

Table 3.8: Specific surface area and pore volume obtained from BET measurements, as well as lattice parameters and unit cell volume derived from X-ray diffraction for ZnO:Ce samples.

Sample	$S_{BET}{}^a$ / m^2/g	Vp^b / cm^3/g	a=b / Å	C / Å	V / $Å^3$
ZnO:Ce0	6.94	0.018	3.242	5.182	47.16733
ZnO:Ce0.2	9.10	0.025	3.242	5.190	47.24015
ZnO:Ce0.4	13.88	0.027	3.247	5.220	47.65988
ZnO:Ce0.6	11.79	0.026	3.248	5.219	47.68011
ZnO:Ce0.8	9.32	0.021	3.245	5.190	47.32762

[a] Specific surface area calculated within the 0.05 – 0.25 range p/p_0.
[b] Total pore volume calculated at $p/p_0 = 0.95$.

The diffraction pattern of undoped and Ce-doped ZnO samples, presented in Figure 3.17a, confirms their structure and crystallinity, while Figure 3.17b shows the band gap energy values calculated using Tauc's equation for all synthesized samples. The samples exhibit a hexagonal wurtzite-type structure, belonging to the $P6_3mc$ (186) space group, in accordance with ICDD 01-070-8072. No diffraction peaks corresponding to secondary phases were detected.

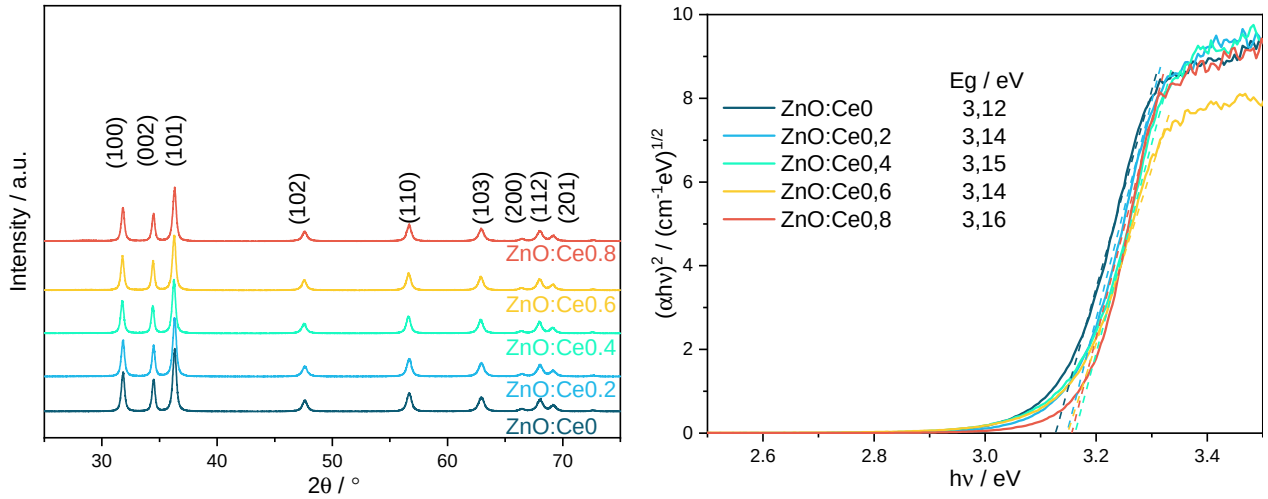

(a) (b)

Figure 3.17: a) XRD patterns of all synthesized samples; b) Tauc plots for the synthesized samples, along with the Eg values, demonstrating the influence of morphology and dopant on the optical and structural properties.

EPR spectroscopy represents an important tool for investigating paramagnetic centers in materials. ZnO is a well-known material that has been extensively characterized by EPR. In the case of undoped ZnO, two distinct signals are typically observed, attributed to two different types of defects, namely zinc vacancies (VZn) and oxygen vacancies (VO), with g parameters of approximately 1.96 and 2.002, respectively [151]. The origin of these two signals can be explained by the core–shell

model [153]. This model suggests that the EPR signal with g $\sim$ 1.96 originates from bulk (core) defects, corresponding to negatively charged zinc vacancies ($VZn^{1-/2-}$). In contrast, the resonance signal with g $\sim$ 2.002 arises from surface (shell) defects, attributed to positively charged oxygen vacancies ($VO^{+/2+}$) (see Figure 3.23).

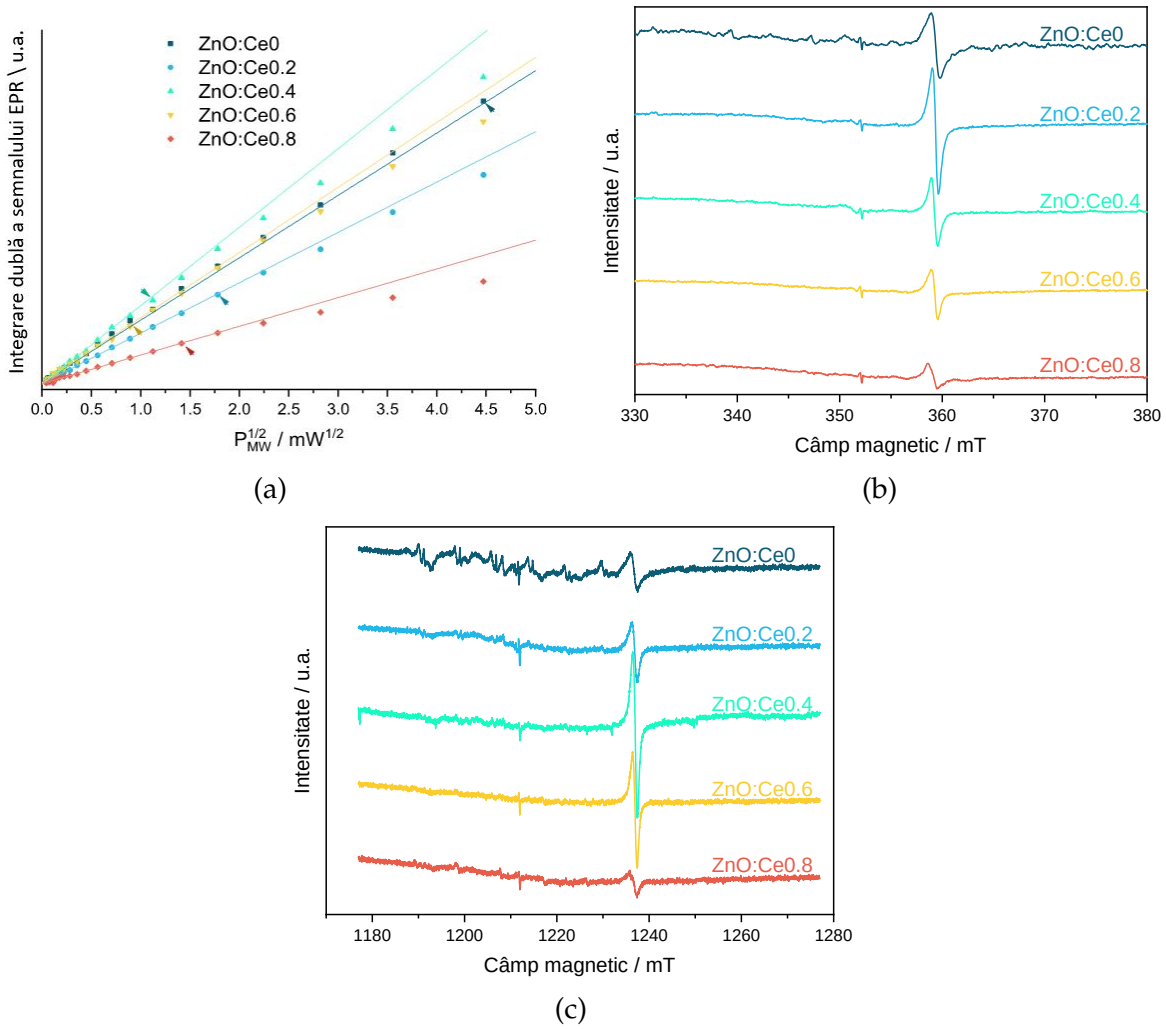

Figura 3.23: a) EPR signal profiles for g = 1.96; b) X-band EPR spectrum; and c) Q-band EPR spectrum of Ce-doped ZnO samples

The X-band EPR spectra of undoped and Ce-doped ZnO samples are shown in Figure 3.23b, exhibiting two distinct resonances: a very intense one at g $\sim$ 1.96 and a less intense one at g $\sim$ 2.002, which are attributed to defect centers in ZnO, as described above. Considering the g values reported in the literature for Ce^{3+}, the first signal could also originate from Ce atoms. Therefore, Q-band EPR measurements were performed to distinguish the signal from negatively charged Zn vacancies from that of Ce^{3+}. The results are presented in Figure 3.23c, where only a single resonance is observed, suggesting that Ce^{3+} ions are not detectable by EPR at room temperature. The g-value of the main transition is independent of dopant concentration, whereas the maximum intensity varies with Ce content, reaching a maximum for ZnO:Ce0.6,

indicating that Ce ions indirectly influence changes in the EPR signal.

Impedance testing is a tool widely used for evaluating the electrochemical performance of supercapacitors (SCs). It allows the observation of the variation of electrical impedance with frequency, providing insight into the characteristics of electrochemical systems [214]. Furthermore, electrochemical interfaces involve interactions occurring between the electrodes and the electrolyte. Impedance analysis also assesses the properties of these interfaces, providing essential data for material selection and design optimization [215]. Figure 3.28 shows the Nyquist plots obtained from the impedance analysis of Ce-doped ZnO. The analysis of the real (Z_{re}) and imaginary ($-Z_{\mathrm{im}}$) components, corresponding to the resistive and reactive parts of the impedance, was essential [216].

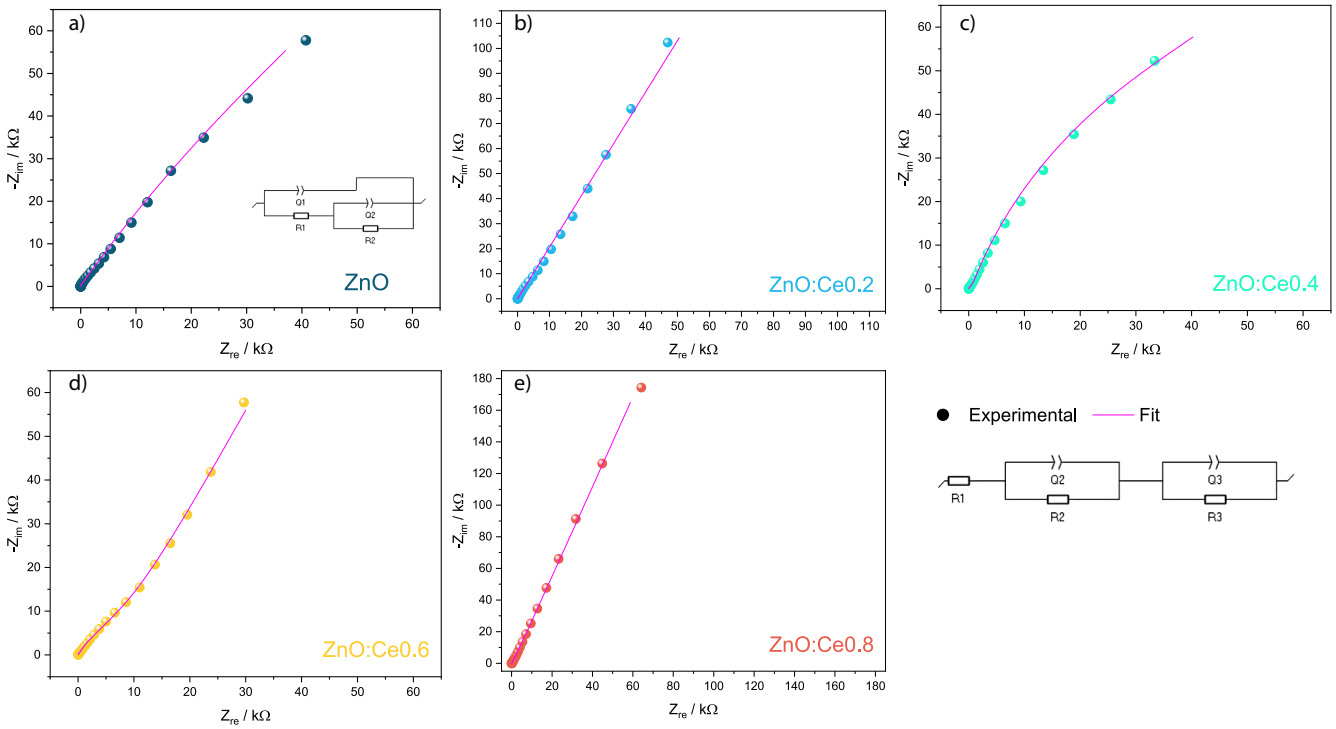

Figura 3.28: Nyquist plots for all supercapacitor designs used to evaluate electrochemical performance. Fitting results demonstrated that Ce doping influences the electrochemical properties of the electrode material.

Examination of the Z_{re} component, corresponding to the resistive part of the impedance, revealed that Ce doping (in the ZnO:Ce0.2 sample) led to a significant increase in resistance. However, as the Ce content increased, the resistance decreased. For the ZnO:Ce0.6 composite, the resistance was even lower than that of pure ZnO. Regarding the $-Z_{im}$ values, which represent the reactive component of the impedance (inductance and capacitance), a similar trend to Z_{re} was observed. It can be concluded that the reactive component of the device using the ZnO:Ce0.6 composite exhibited the lowest value. Increasing the amount of Ce incorporated into ZnO caused a simultaneous increase in resistance and inductance. The data also

indicate that higher Ce concentrations can have adverse effects on supercapacitor performance, likely due to interactions occurring either at the electrode or at the electrode/electrolyte interface. Furthermore, the Nyquist curves of the devices did not display a semicircular shape in the high-frequency region but showed inductive characteristics. An almost linear line in the low-frequency region indicated the capacitive behavior of devices using ZnO and ZnO:Ce as electrodes.

Figure 3.29a illustrates the time-dependent variation of the applied voltage during the charging and discharging process. Undoped ZnO exhibits an almost triangular shape, with no observable drops due to internal resistance. However, the introduction of Ce leads to the appearance of internal resistance drops at the maximum voltage during discharge. All configurations display an almost triangular shape, indicating the presence of double-layer capacitance.

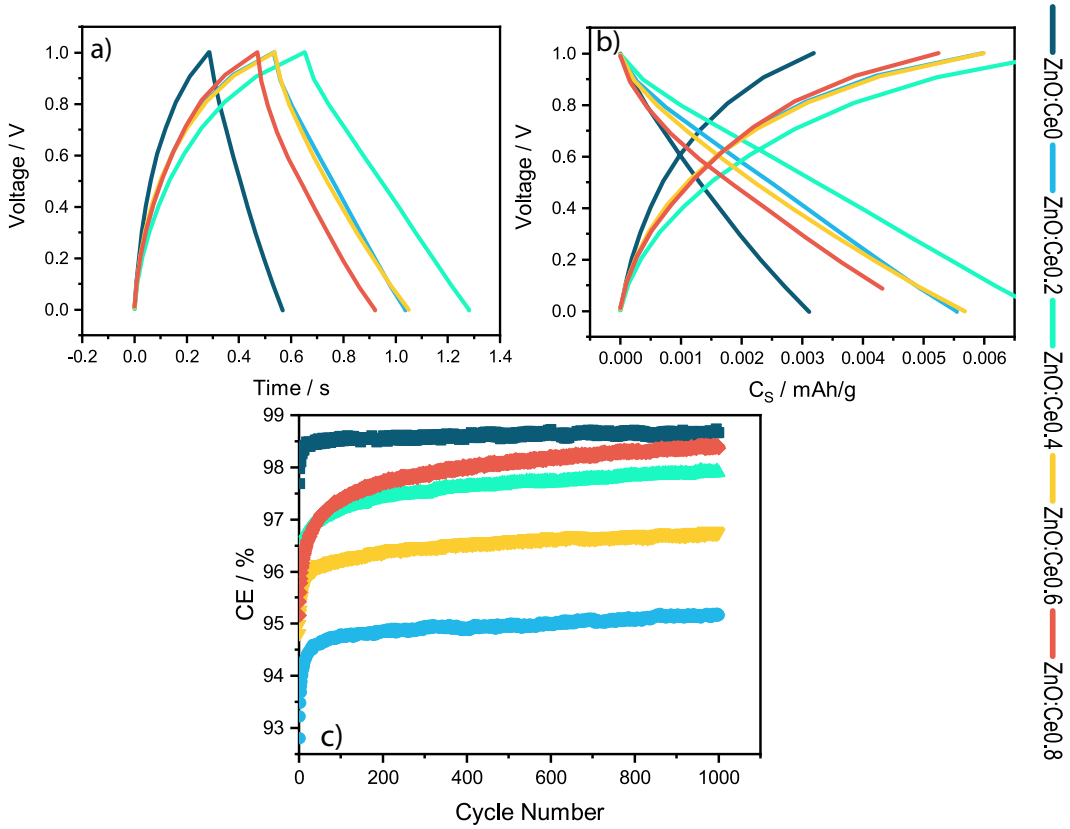

Figura 3.29: a) Galvanostatic charge–discharge curves for the tested SCs, indicating the presence of electric double-layer capacitive behavior; b) potential versus specific capacity of the SCs, showing increased specific capacity for the ZnO:Ce0.4 and ZnO:Ce0.6 samples; c) capacity retention after 1000 cycles, demonstrating good stability for all tested devices.

This observation is consistent with the CV analysis results, as the CV study also revealed an almost rectangular shape, which reflects the behavior of the capacitance associated with the electric double layer.

The EPR analysis indicated that the ZnO:Ce0.6 sample exhibits the highest con-

centration of paramagnetic centers and that the Ce ions directly influence the defect centers associated with Zn by modifying their relaxation time. The PL analysis showed a clear variation in emissions correlated with the Ce doping concentration, this balance being essential for maximizing the electrochemical performance of the sample. Impedance analysis revealed that the sample doped with 0.6% Ce exhibits low ohmic resistance and low inductance. Consequently, it was determined that the ZnO:Ce0.6 sample demonstrates favorable performance as an electrode material, and the Ce content of 0.6% was identified as the optimal doping level, based on favorable electrochemical properties and defect structure.

3.2.3 Conclusions

- Doping ZnO with an optimal percentage of Ce leads to competitive electrochemical performance for supercapacitor applications.
- The synthesized nanoparticles have a nano-flower like morphology, confirmed by SEM and TEM analyses.
- X-ray diffraction (XRD) confirmed the incorporation of Ce ions into the ZnO crystal lattice.
- XPS analysis revealed the presence of Ce^{3+} and Ce^{4+} ions, with a higher concentration of Ce^{3+} ions at the surface of the nanoparticles.
- EPR spectroscopy confirmed the presence of Zn-associated defects and positively charged oxygen vacancies, as well as the influence of Ce doping on these defect centers. The ZnO:Ce0.6 sample exhibits the highest concentration of paramagnetic centers.
- PL measurements showed that the concentration of intrinsic ZnO defects changes with increasing Ce content, indicating a balance essential for maximizing electrochemical performance.
- The electrochemical performance of the materials was evaluated through CV, EIS, and GCD tests, confirming the superiority of the ZnO:Ce0.6 sample.
- The ZnO:Ce0.6 sample exhibited a capacity retention of approximately 95% after 1000 cycles, indicating high electrochemical stability and good reproducibility.
- Doping ZnO with Ce enhances electrochemical performance by increasing ionic diffusivity and optimizing the capacitive contributions of the material.

3.3 g-C_3N_4-ZnO:Cu-based Nanocomposites for Supercapacitor Applications

The results obtained from the EDS analysis are presented in Figure 3.32, which highlighted the elements Zn, O, Cu, C, and N, confirming the formation of Cu–ZnO nanoparticles deposited on thin layers of g-C_3N_4.

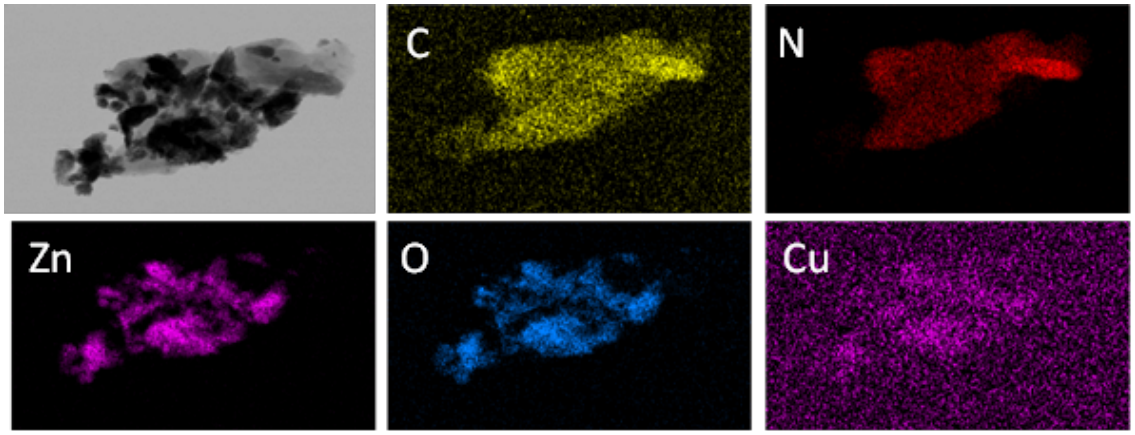

Figure 3.32: The presence of C, N, Zn, O, and Cu in the g-C_3N_4–ZnO:Cu samples as evidenced by EDS.

The study of the optical properties of g-C_3N_4–ZnO:Cu nanoparticles was carried out through optical absorption measurements using UV–Vis spectroscopy. Figure 3.34a presents the absorption spectra for g-C_3N_4-ZnO doped with different Cu concentrations, with an absorption maximum located around 350 nm. A slight shift in the position of the absorption maximum was observed with increasing Cu concentration in ZnO.

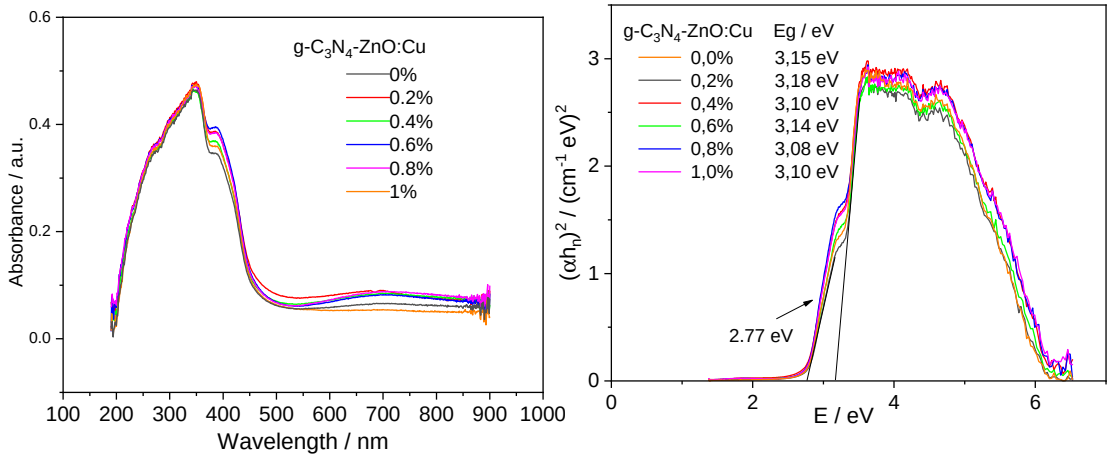

(a) (b)

Figure 3.34: a) UV–Vis spectrum of the g-C_3N_4-ZnO:Cu nanocomposite materials; b) Graphical representation of the Tauc equation, as well as the Eg values

The band gap energy (Eg) of the g-C_3N_4-ZnO:Cu composites was estimated based on the Tauc equation:

$$\sqrt[n]{\alpha h\nu} = A(h\nu - E_g)$$

In this equation, α is the absorption coefficient, $h\nu$ is the photon energy, A is a constant, and n is the Tauc exponent, which depends on the type of electronic transition (for example, $n = 2$ for allowed indirect transitions and $n = \frac{1}{2}$ for allowed direct transitions). To determine E_g, a plot of $(\alpha h\nu)^{1/n}$ versus $h\nu$ was constructed, and the linear portion of the curve was extrapolated to the x-axis; the resulting intersection corresponds to the band gap energy E_g.

Figure 3.34b presents the corresponding Tauc plots, along with the band gap energy values for all samples, showing a slight decrease with increasing copper doping. The reduction in band gap energy is attributed to the strong sp–d exchange interaction between the ZnO band electrons and the localized d electrons of Cu^{2+} ions that substitute Zn^{2+} ions, leading to a shift of the Fermi level toward the valence band. In the undoped state, the Fermi level is located at the center of the band gap, and its position depends on the type of semiconductor [226]. Doping with Cu ions modifies the electrical and optical properties of the semiconductor by introducing acceptor levels near the valence band. These levels facilitate the excitation of electrons from the valence band, increasing the hole concentration and enhancing p-type conductivity. Cu doping often results in a slight decrease in the band gap energy due to the formation of localized states and the intensification of electron–hole interactions. These results are consistent with other studies reported in the literature, which have confirmed that with increasing Cu dopant concentration, the optical band gap energy of Cu-doped ZnO decreases [236].

The peaks observed at 2θ = 12.71°and 27.47°are attributed to the (100) and (002) planes of g-C_3N_4 (JCPDS XXX 79–0208), while all other peaks correspond to the hexagonal wurtzite structure of ZnO ($P6_{3mc}$, JCPDS 79–0208). No additional crystalline phases were identified, confirming the purity of the samples. The unit cell parameters were calculated from the Rietveld refinements and are presented in Table 3.12. This table also includes the average crystallite size values determined using the Williamson–Hall method. Upon doping with Cu ions, the unit cell volume slightly increases up to 0.8% Cu, followed by a significant decrease at higher Cu content (1.0%). The increase in unit cell volume is somewhat unexpected, as Cu^{2+} ions (0.73 Å) have an ionic radius similar to that of Zn^{2+} ions (0.74 Å). This behavior may be explained by the fact that some Cu^{2+} ions partially substitute Zn^{2+} ions, while others occupy interstitial positions. These interstitial positions generate various lattice defects, such as Zn interstitials or oxygen vacancies. At a molar concentration of 1.0%

Cu, a significant reduction in unit cell volume is observed, likely due to the segregation of Cu^{2+} ions at the ZnO surface and the formation of zinc vacancies. The average crystallite size shows very little variation, ranging between 11 and 14 nm.

Table 3.12: Unit cell parameters, unit cell volume, and average crystallite size for the g-C_3N_4-ZnO:Cux% samples

Sample	ZnO:Cu				g-C_3N_4		
g-C_3N_4-ZnO:	$a = b$ (Å)	c (Å)	V (Å^3)	D (nm)	$a = b = c$ (Å)	c (Å)	V (Å^3)
Cu0.0	3.243	5.199	47.37	12	6.492	2.516	91.8
Cu0.2	3.243	5.202	47.39	11	6.492	2.516	91.8
Cu0.4	3.246	5.196	47.39	12	6.492	2.516	91.8
Cu0.6	3.247	5.196	47.40	14	6.492	2.516	91.8
Cu0.8	3.243	5.199	47.36	10	6.492	2.516	91.8
Cu1.0	3.241	5.195	47.26	13	6.492	2.516	91.8

Additional information regarding the structure and the presence of defects or impurities in the material was obtained through photoluminescence (PL). The PL emission spectra were recorded at an excitation wavelength of 325 nm. All samples exhibit similar spectra, showing a broad emission band in the 400–750 nm range. To better highlight the emission bands and enable a more accurate assignment, deconvolution of the experimental spectra obtained for the g-C_3N_4-ZnO:Cu composite samples was performed. Since the graphs show a high degree of similarity, both the undoped nanocomposite and the one doped with 1% Cu are illustrated in Figure 3.36.

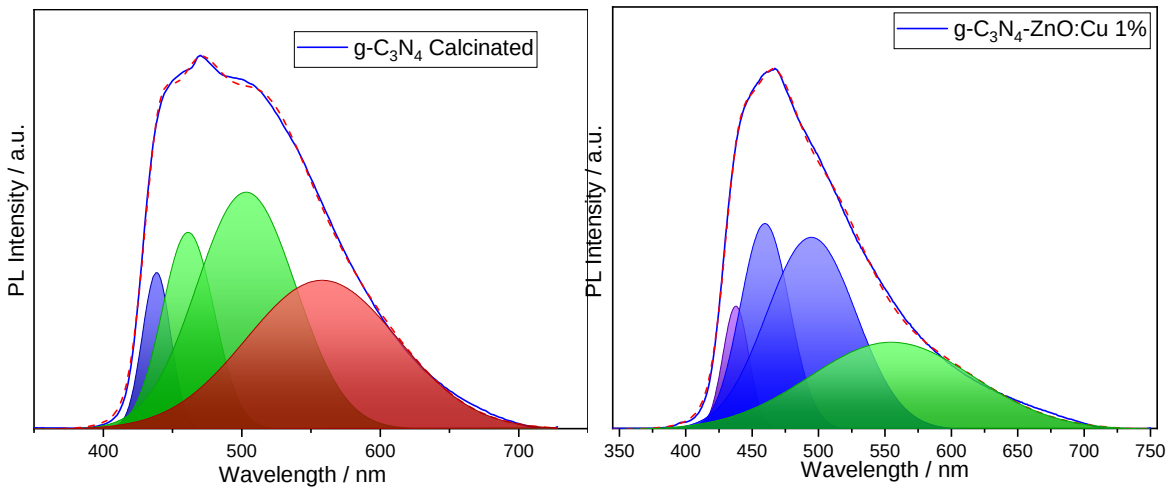

Figura 3.36: Deconvolution of the PL spectra for: a) g-C_3N_4-ZnO and b) g-C_3N_4-ZnO:Cu1.0.

Qualitative and quantitative compositional analysis by XPS was performed for the g-C_3N_4-ZnO:Cu0.8 sample, and the results are presented in Figures 3.37a–d. The XPS spectra of the Zn 2p core-level doublet are shown in Figure 3.37a. The doublet located at 1021.7 eV (2p3/2) and 1044.8 eV (2p1/2) is characteristic of the binding energy typical for Zn^{2+}. In addition, two satellite peaks at higher binding energies were included in the deconvolution process.

The XPS spectrum of the Cu $2p_{3/2}$ core level is presented in Figure 3.37b. The main peak is located at 932.7 eV, and the calculated Cu/Zn ratio is 0.008, indicating a good doping efficiency and the presence of Cu^{2+} ions, as expected, without additional oxidation states.

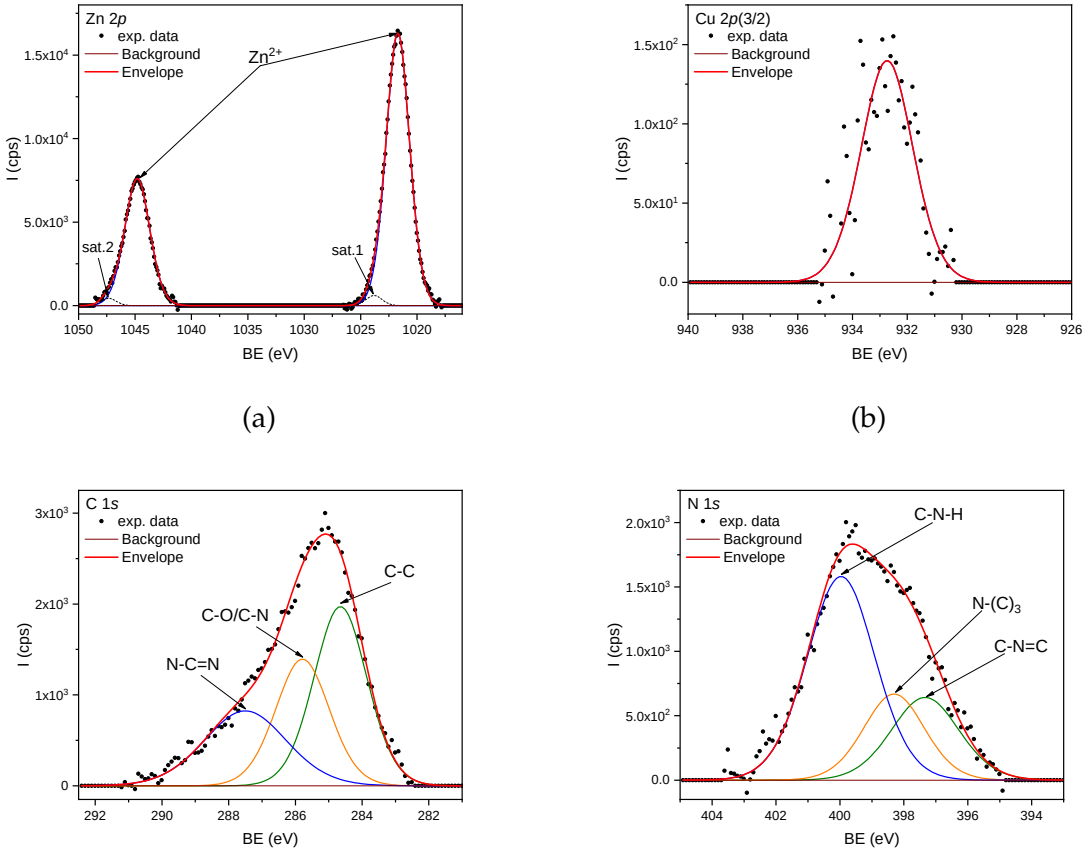

Figure 3.37: XPS analysis of the g-C_3N_4-ZnO:Cu0.8% sample: a) Zn 2p core-level doublet; b) Cu $2p_{3/2}$ core level; c) C 1s core level; d) N 1s core level.

To observe the contribution of diffusive and capacitive phenomena in the energy storage process of the Cu-doped sample, a Dunn analysis was performed for the device with the best performance, g-C_3N_4-ZnO:Cu0.8% (Figure 3.42) [250]. The equation used to calculate the contributions is expressed as:

$$I(v) = k_1 v + k_2 \sqrt{v}$$

where k_1 represents the capacitive current, k_2 represents the diffusive current, and v is the scan rate. The relative contributions of each mechanism can be quantified by analyzing the slope and intercept of the Dunn plot.

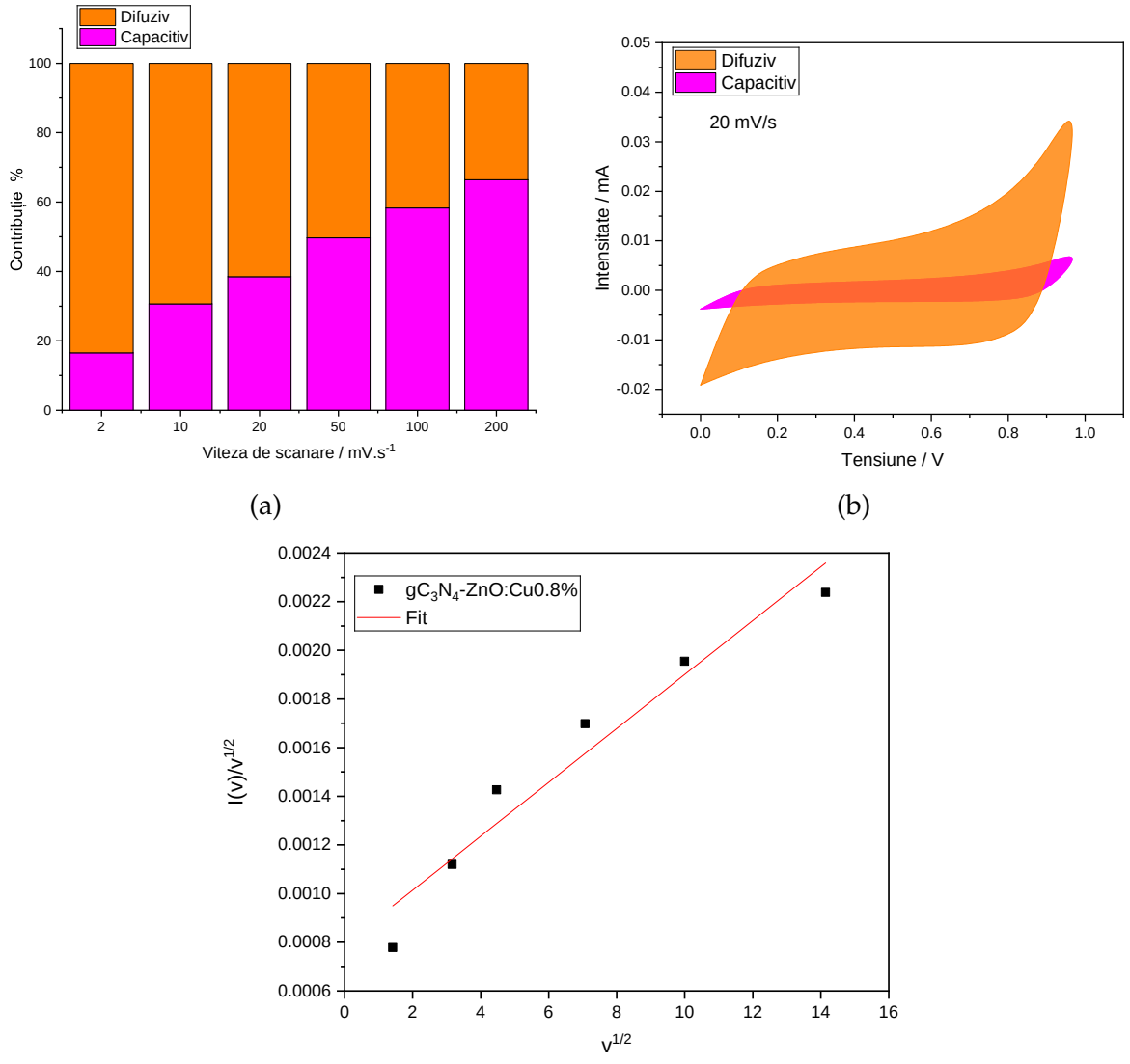

Figure 3.42: Dunn method for the g-C_3N_4-ZnO:Cu0.8 sample illustrating: a) the percentage of capacitive and diffusive contributions at different scan rates; b) CV representation of capacitive and diffusive process contributions; c) linear fitting used to obtain the slope and intercept values.

Figure 3.42a shows the percentage contribution of capacitive and diffusive processes at different scan rates. Figure 3.42b presents the CV representation of the diffusive and capacitive contributions at a scan rate of 20 mV/s, while Figure 3.42c illustrates the linear fitting used to obtain the slope and intercept values on the x-axis, from which the capacitive and diffusive contributions were calculated. The Dunn analysis complements the CV results very well, as it also indicates that charge storage involves both capacitive and diffusive phenomena at each scan rate. The results suggest that the charge storage mechanism transitions from EDLC dominance at high scan rates to an increased pseudocapacitive contribution at low scan rates. As the scan rate decreases, the diffusive contribution extracted from the Dunn analysis becomes more significant, indicating that ion transport within the pores and toward faradaic active sites increasingly contributes to charge storage. Consequently, the CV profiles become more rectangular at lower scan rates, as ions have sufficient time to penetrate the pores and access redox-active sites. This improved ionic accessibility enables more complete and reversible faradaic reactions, resulting in a more uniform capacitive behavior closer to the ideal case, demonstrating that pseudocapacitive processes dominate the overall charge storage mechanism at low scan rates [246], [247].

3.3.3 Conclusions

- g-C_3N_4-ZnO:Cu nanocomposites were investigated as electrode materials for supercapacitors.
- SEM and TEM analyses revealed the uniform distribution of ZnO:Cu NF within the g-C_3N_4 layers.
- XPS and EPR spectroscopy confirmed the incorporation of copper and its +2 oxidation state within the material structure.
- Cu doping introduces additional defects in the ZnO lattice through substitutional or interstitial incorporation, influencing the structural and optical properties of the material.
- The obtained nanocomposites exhibit a crystalline structure, with particle sizes ranging between 11 and 14 nm.
- Cu doping leads to a reduction of the band gap energy from 3.15 eV to 3.08 eV.
- Electrochemical analysis revealed a charge storage mechanism resulting from the synergistic contribution of EDLC-type and pseudocapacitive behavior.

- Cu doping enhances electrical conductivity and increases the number of active sites available for electrochemical reactions.
- The g-C_3N_4-ZnO:Cu0.8-based device exhibited the best electrochemical performance: a maximum specific capacitance of 181.8 F/g, an energy density of 25.24 Wh/kg, and a power density of 917.81 W/kg.
- The material demonstrated excellent electrochemical stability, retaining 110% capacity after 10,000 cycles.
- The ratio between carbon-based defect centers in g-C_3N_4 and the concentration of Cu^{2+} ions in ZnO plays a crucial role in electrochemical performance.
- Defect engineering has been identified as a key factor in optimizing electrode materials for supercapacitors.
- The obtained results demonstrate the high potential of Cu-doped ZnO combined with carbon-based materials such as g-C_3N_4 for the development of future energy storage devices.

5. General Conclusions

- Supercapacitors represent a promising direction in the field of energy storage due to their rapid charging capability, significantly longer lifespan compared to conventional batteries, and ability to deliver energy instantaneously.

- The use of zinc oxide (ZnO)-based materials for supercapacitor electrodes represents a promising solution due to their favorable electrochemical properties, such as good conductivity, chemical stability, and low cost. Nanoscale ZnO structures (nanowires, nanoparticles, thin films) can increase the active surface area of the electrode, enhancing storage capacity and overall supercapacitor performance, thereby supporting the development of more efficient and affordable energy storage systems.

- ZnO materials with various morphologies can be synthesized by hydrothermal, solvothermal, or chemical precipitation methods, where morphology directly influences the structural, optical, and electrochemical properties. Depending on the synthesis method used, five distinct ZnO morphologies were obtained: nano-rods, pyramidal, hexagonal, conical, and nano-flower-shaped structures.

- Structural and morphological analyses were performed using X-ray diffraction (XRD), scanning electron microscopy (SEM), and X-ray photoelectron spectroscopy (XPS). Electron spin resonance (EPR) spectroscopy and photoluminescence (PL) spectroscopy were used to investigate dopant-induced defect structure modifications, while electrochemical measurements were carried out by testing them in symmetric "all-in-one" supercapacitor (SC) devices for each sample.

- The nano-flower morphology proved to be optimal for doping processes and for integration with carbon-based structures, leading to superior electrochemical performance.

- The ratio between zinc and oxygen vacancies represents a key parameter in determining energy storage performance in ZnO-based materials.

- Ce doping in ZnO leads to modification of the defect structure and optimization of electrochemical properties, with the ZnO:Ce0.6 sample exhibiting the best performance.
- g-C_3N_4-ZnO:Cu nanocomposites exhibit a uniform distribution of nanoparticles and improved electrical conductivity due to Cu doping. g-C_3N_4 was obtained by thermal decomposition of urea, while the deposition of ZnO:Cu onto the g-C_3N_4 carbon structure was achieved using the polyallylamine hydrochloride (PAH) binding polymer.
- The supercapacitor device based on g-C_3N_4-ZnO:Cu0.8 exhibited high electrochemical performance, with a specific capacitance of 181.8 F/g, an energy density of 25.24 Wh/kg, and a power density of 917.81 W/kg.
- The developed materials demonstrated excellent electrochemical stability, showing an energy storage capacity increase of up to 110% after 10,000 cycles.
- Defect engineering and morphology control represent key factors in optimizing electrode materials for supercapacitor applications and modern energy storage systems.

References

[1] D. Maradin, "Advantages and disadvantages of renewable energy sources utilization," *International Journal of Energy Economics and Policy*, 11, (3), 176–183, 2021.

[2] Q. Zhu, W. Sun, H. Zhou, and D. Mao, "A review of lithium–sulfur batteries based on metal–organic frameworks: Progress and prospects," *Batteries*, 11, (3), 89, 2025.

[3] J. Li, P. Sanglier, H. Qu, Z. Miao, Y. Li, and B.-L. Su, "Photo-assisted lithium–oxygen batteries: Mechanisms, materials, and perspectives," *Advanced Materials*, e18355, 2025.

[4] Z. Li, S. Cui, J. H¨acker, M. Nojabaee, M. Fichtner, G. Cui, and Z. Zhao-Karger, "Calcium chemistry as a new member of post-lithium battery family: What can we learn from sodium and magnesium systems," *Angewandte Chemie International Edition*, 64, (5), e202415942, 2025.

[5] M. Eltaweel, N. A. Mostafa, C. Kalyvas, Y. Chen, and M. R. Herfatmanesh, "Optimising flywheel energy storage systems for enhanced windage loss reduction and heat transfer: A computational fluid dynamics and anova-based approach," *Energy Reports*, 13, 834–855, 2025.

[6] A. F. Kilicaslan and I. Dincer, "Design and performance assessment of an integrated energy system with compressed air and pumped hydro storage," *Journal of Energy Storage*, 116, 116039, 2025.

[7] S. Ahn, A. Yun, D. Ko, V. Singh, J. M. Joo, and H. R. Byon, "Organic redox flow batteries in non-aqueous electrolyte solutions," *Chemical Society Reviews*, 2025.

[8] H. Xu, X. Han, W. Hua, D. Friedrich, G. Santori, E. Bevan, K. Vafai, F. Wang, X. Zhang, G. Yu, et al., "Progress on thermal storage technologies with high heat density in renewables and low carbon applications: Latent and ther- mochemical energy storage," *Renewable and Sustainable Energy Reviews*, 215, 115587, 2025.

[9] M. Hahn, R. K¨otz, R. Gallay, and A. Siggel, "Pressure evolution in propylene carbonate based electrochemical double layer capacitors," *Electrochimica Acta*, 52, (4), 1709–1712, 2006.

[10] J. Libich, J. Máca, J. Vondrák, O. Čech, and M. Sedlaříková, "Supercapacitors: Properties and applications," *Journal of energy storage*, 17, 224–227, 2018.

[11] N. Nadiah, F. S. Omar, A. Numan, Y. Mahipal, S. Ramesh, and K. Ramesh, "Influence of acrylic acid on ethylene carbonate/dimethyl carbonate based liquid electrolyte and its supercapacitor application," *International Journal of Hydrogen Energy*, 42, (52), 30683–30690, 2017.

[12] S. Samantaray, D. Mohanty, I.-M. Hung, M. Moniruzzaman, and S. K. Sat pathy, "Unleashing recent electrolyte materials for next-generation supercapacitor applications: a comprehensive review," *Journal of Energy Storage*, 72, 108352, 2023.

[13] A. Shukla, S. Sampath, and K. Vijayamohanan, "Electrochemical supercapacitors: Energy storage beyond batteries," *Current science*, 79, (12), 1656–1661, 2000.

[14] N. I. Jalal, R. I. Ibrahim, and M. K. Oudah, "A review on supercapacitors: Types and components," *Journal of physics: conference series*, 1973, 012015, IOP Publishing, 2021.

[15] J. Kang, J. Wen, S. H. Jayaram, A. Yu, and X. Wang, "Development of an equi valent circuit model for electrochemical double layer capacitors (edlcs) with distinct electrolytes," *Electrochimica Acta*, 115, 587–598, 2014.

[16] J. Wang, J. Polleux, T. Brezesinski, S. Tolbert, and B. Dunn, "The pseudocapacitance behaviors of TiO_2 (anatase) nanoparticles," *ECS Transactions*, 11, (31), 101, 2008.

[17] B. Saravanakumar, S. Ramachandran, G. Ravi, V. Ganesh, S. Ravichandran, P. Muthu Mareeswaran, and R. Yuvakkumar, "Enhanced pseudocapacitive performance of SnO_2, Zn-SnO_2, and Ag-SnO_2 nanoparticles," *Ionics*, 24, 4081 4092, 2018.

[18] M. Xu, L. Kong, W. Zhou, and H. Li, "Hydrothermal synthesis and pseudo capacitance properties of -MnO_2 hollow spheres and hollow urchins," *The Journal of Physical Chemistry C*, 111, (51), 19141–19147, 2007.

[19] S. Wen, J.-W. Lee, I.-H. Yeo, J. Park, and S.-i. Mho, "The role of cations of the electrolyte for the pseudocapacitive behavior of metal oxide electrodes, MnO_2

and RuO_2," *Electrochimica Acta*, 50, (2-3), 849–855, 2004.

[20] M. Liu, J. Chang, J. Sun, and L. Gao, "A facile preparation of NiO/Ni compo sites as high-performance pseudocapacitor materials," *RSC advances*, 3, (21), 8003–8008, 2013.

[21] C. T. Altaf, O. Coskun, A. Kumtepe, A. M. Rostas, I. Iatsunskyi, E. Coy, E. Er dem, M. Sankir, and N. D. Sankir, "Photo-supercapacitors based on nanoscaled ZnO," *Scientific reports*, 12, (1), 11487, 2022.

[22] D. P. Chatterjee and A. K. Nandi, "A review on the recent advances in hybrid supercapacitors," *Journal of Materials Chemistry A*, 9, (29), 15880–15918, 2021.

[23] H. Li, U. Naeem, P.-J. Li, L.-J. Wu, H.-W. Yue, A. Alshoaibi, D. Wang, B. De ghfel, S. Kheawhom, and A. A. Mohamad, "Structural analysis by x-ray di ffraction technique of transition metal doped zinc oxide and its applications in energy storage systems: A critical review," *International Journal of Energy Research*, 2025, (1), 2587682, 2025.

[24] R. Yadav, S. Sharma, H. Borkar, and K. Kumari, "Zinc oxide-enhanced porous activated carbon from waste walnut shells for supercapacitor electrodes," *Energy Storage*, 7, (3), e70154, 2025.

[25] E. Ercay, S. Ersoy, M. Ozcan, F. B. Misirlioglu, A. Gungor, A. Ozarowski, F. Kaya, A. M. Rostas, C. Kaya, and E. Erdem, "Enhancing ZnO-based su percapacitors through carbon-induced defect centers," *MRS Bulletin*, 50, (5), 572–584, 2025.

[26] M. S. Whittingham, "History, evolution, and future status of energy storage," *Proceedings of the IEEE*, 100, (Special Centennial Issue), 1518–1534, 2012.

[27] S.-x. Yan, S.-h. Luo, J. Feng, L. Yang, P.-w. Li, Q. Wang, Y.-h. Zhang, X. Liu, and L.-j. Chang, "Asymmetric, flexible supercapacitor based on Fe–Co alloy@sulfide with high energy and power density," *ACS Applied Materials & Interfaces*, 13, (42), 49952–49963, 2021.

[28] M. E. S¸ahin, F. Blaabjerg, and A. Sangwongwanich, "A comprehensive review on supercapacitor applications and developments," *Energies*, 15, (3), 674, 2022.

[29] S.-x. Yan, S.-h. Luo, H. Liu, L. Yang, Q. Wang, Y.-h. Zhang, and X. Liu, "In-situ partial reduction-sulfurized Fe_3O_4@FeS based on pickling iron red as a versatile electrode for high-performance lithium ion batteries and supercapacitor devices," *Surface and Coatings Technology*, 429, 127980, 2022.

[30] G. M. Di Mari, G. Mineo, G. Franz'o, S. Mirabella, E. Bruno, and V. Strano,

"Low-cost, high-yield ZnO nanostars synthesis for pseudocapacitor applications," *Nanomaterials*, 12, (15), 2588, 2022.

[31] A. Falamas, I. Marica, A. Popa, D. Toloman, S. Pruneanu, F. Pogacean, F. Nek vapil, T. D. Silipas, and M. Stefan, "Size-dependent spectroscopic insight into the steady-state and time-resolved optical properties of ZnO photocatalysts," *Materials Science in Semiconductor Processing*, 145, 106644, 2022.

[32] A. Popa, D. Toloman, M. Stan, M. Stefan, T. Radu, G. Vlad, S. Ulinici, G. Bai san, S. Macavei, L. Barbu-Tudoran, et al., "Tailoring the RhB removal rate by modifying the pvdf membrane surface through ZnO particles deposition," *Journal of Inorganic and Organometallic Polymers and Materials*, 31, 1642–1652, 2021.

[33] T. D. T. Ung, T. K. C. Tran, T. N. Pham, D. N. Nguyen, D. K. Dinh, and Q. L. Nguyen, "Cdte and cdse quantum dots: synthesis, characterizations and applications in agriculture," *Advances in Natural Sciences: Nanoscience and Nanotechnology*, 3, (4), 043001, 2012.

[34] S.-H. Feng and G.-H. Li, "Hydrothermal and solvothermal syntheses," in Modern inorganic synthetic chemistry, 73–104, *Elsevier*, 2017.

[35] A. Rabenau, "The role of hydrothermal synthesis in preparative chemistry," *Angewandte Chemie International Edition in English*, 24, (12), 1026–1040, 1985.

[36] M. Yoshimura and K. Byrappa, "Hydrothermal processing of materials: past, present and future," *Journal of Materials Science*, 43, 2085–2103, 2008.

[37] V. Teske, E. Vogel, and E. Bich, "Viscosity measurements on water vapor and their evaluation," *Journal of Chemical & Engineering Data*, 50, (6), 2082–2087, 2005.

[38] K. Heger, M. Uematsu, and E. Franck, "The static dielectric constant of water at high pressures and temperatures to 500 mpa and 550 c," *Berichte der Bunsengesellschaft für physikalische Chemie*, 84, (8), 758–762, 1980.

[39] E. Araujo-Lopez, J. S. Lopez-Echeverry, and S. Reif-Acherman, "The Antoine equation of state: Rediscovering the potential of an almost forgotten expression for calculating volumetric properties of pure compounds," *Chemical Engineering Science*, 177, 89–109, 2018.

[40] J. Xie, H. Wang, M. Duan, and L. Zhang, "Synthesis and photocatalysis properties of ZnO structures with different morphologies via hydrothermal method," *Applied surface science*, 257, (15), 6358–6363, 2011.

[41] A. N. P. Madathil, K. Vanaja, and M. Jayaraj, "Synthesis of ZnO nanoparticles by hydrothermal method," *Nanophotonic materials IV*, 6639, 47–55, SPIE, 2007.

[42] Y. Zhang, M. K. Ram, E. K. Stefanakos, and D. Y. Goswami, "Synthesis, characterization, and applications of ZnO nanowires," *Journal of Nanomaterials*, 2012, (1), 624520, 2012.

[43] Y. Dahman, Nanotechnology and functional materials for engineers. *Elsevier*, 2017.

[44] Z. Sun and R. Sköld, "A multi-parameter titration method for the determination of formation ph for metal hydroxides," *Minerals engineering*, 14, (11), 1429–1443, 2001.

[45] D. Bokov, A. Turki Jalil, S. Chupradit, W. Suksatan, M. Javed Ansari, I. H. Shewael, G. H. Valiev, and E. Kianfar, "Nanomaterial by sol-gel method: synthesis and application," *Advances in materials science and engineering*, 2021, (1), 5102014, 2021.

[46] J. Ansari, W. Suksatan, I. Shewael, D. Bokov, E. Kianfar, S. Chupradit, G. Va liev, et al., "Nanomaterial by sol-gel method: Synthesis and application,"

[47] R. Verma, B. Mantri, A. K. Srivastava, et al., "Shape control synthesis, cha racterizations, mechanisms and optical properties of larg scaled metal oxide nanostructures of ZnO and TiO_2," *Advanced Materials Letters*, 6, (4), 324–333, 2015.

[48] R. Vijayalakshmi and V. Rajendran, "Synthesis and characterization of nano TiO_2 via different methods," *Archives of Applied Science Research*, 4, (2), 1183–1190, 2012.

[49] J. Hasnidawani, H.N.Azlina, H.Norita, N.Bonnia, S.Ratim, andE.Ali, "Synthesis of ZnO nanostructures using sol-gel method," *Procedia chemistry*, 19, 211-216, 2016.

[50] Ö. A. Yıldırım and C. Durucan, "Synthesis of zinc oxide nanoparticles elaborated by microemulsion method," *Journal of Alloys and Compounds*, 506, (2), 944–949, 2010.

[51] A. M. Pineda-Reyes and M. d. l. L. Olvera, "Synthesis of ZnO nanoparticles from water-in-oil (w/o) microemulsions," *Materials chemistry and physics*, 203, 141–147, 2018.

[52] X. Li, G. He, G. Xiao, H. Liu, and M. Wang, "Synthesis and morphology con trol of ZnO nanostructures in microemulsions," *Journal of Colloid and Interface*

Science, 333, (2), 465–473, 2009.

[53] Y. Wang, X. Zhang, A. Wang, X. Li, G. Wang, and L. Zhao, "Synthesis of ZnO nanoparticles from microemulsions in a flow type microreactor,"*Chemical Engineering Journal*, 235, 191–197, 2014.

[54] D. P. Norton, Y. Heo, M. Ivill, K. Ip, S. Pearton, M. F. Chisholm, and T. Steiner, "ZnO: growth, doping & processing," *Materials today*, 7, (6), 34–40, 2004.

[55] A. U. Ammar, M. Stefan, S. G. Macavei, S. Tripon, O. Pana, C. Leostean, I. D. Vlaicu, A. M. Rostas, and E. Erdem, "Characterization of defect structures in nanoscaled W-doped TiO_2 tested as supercapacitor electrode materials," *Journal of Materials Science: Materials in Electronics*, 34, (2), 98, 2023.

[56] A.Sulciute, K.Nishimura, E.Gilshtein, F.Cesano, G.Viscardi, A.G.Nasibulin, Y. Ohno, and S. Rackauskas, "ZnO nanostructures application in electroche mistry: influence of morphology," *The Journal of Physical Chemistry C*, 125, (2), 1472–1482, 2021.

[57] A. B. G. Trabelsi, R. Nasser, F. H. Alkallas, A. F. B. Saqr, B. El-Gammal, J. M. Song, and H. Elhouichet, "Tuning the electrochemical properties of ZnO through chromium doping and its suitability for supercapacitor application," *Journal of Energy Storage*, 87, 111487, 2024.

[58] Y. WuandC.Cao,"The way to improve the energy density of supercapacitors: Progress and perspective," *Science China Materials*, 61, (12), 1517–1526, 2018.

[59] P. Simon and Y. Gogotsi, "Materials for electrochemical capacitors," *Nature materials*, 7, (11), 845–854, 2008.

[60] L. Wang, H. Ji, S. Wang, L. Kong, X. Jiang, and G. Yang, "Preparation of Fe_3O_4 with high specific surface area and improved capacitance as a supercapacitor," *Nanoscale*, 5, (9), 3793–3799, 2013.

[61] A. U. Ammar, I. D. Yildirim, F. Bakan, and E. Erdem, "ZnO and mxenes as electrode materials for supercapacitor devices," *Beilstein Journal of Nanotech nology*, 12, (1), 49–57, 2021.

[62] M. D. Angelin, S. Rajkumar, J. P. Merlin, A. R. Xavier, M. Franklin, and A. Ra vichandran, "Electrochemical investigation of Zr-doped ZnO nanostructured electrode material for high-performance supercapacitor," *Ionics*, 26, 5757 5772, 2020.

[63] I. N. Reddy, C. V. Reddy, A. Sreedhar, J. Shim, M. Cho, K. Yoo, and D. Kim, "Structural, optical, and bifunctional applications: Supercapacitor and photo-

electrochemical water splitting of Ni-doped ZnO nanostructures," *Journal of Electroanalytical Chemistry*, 828, 124–136, 2018.

[64] I. Shaheen, I. Hussain, T. Zahra, M. S. Javed, S. S. A. Shah, K. Khan, M. B. Ha nif, M. A. Assiri, Z. Said, W. U. Arifeen, et al., "Recent advancements in metal oxides for energy storage materials: design, classification, and electrodes configuration of supercapacitor," *Journal of Energy Storage*, 72, 108719, 2023.

[65] G. Yu, X. Xie, L. Pan, Z. Bao, and Y. Cui, "Hybrid nanostructured materials for high-performance electrochemical capacitors," *Nano Energy*, 2, (2), 213–234, 2013.

[66] Y. Wang, Y. Liu, and J. Zhang, "Colloid electrostatic self-assembly synthesis of SnO_2/graphene nanocomposite for supercapacitors," *Journal of Nanoparticle Research*, 17, 1–10, 2015.

[67] M. Ramezani, M. Fathi, and F. Mahboubi, "Facile synthesis of ternary MnO_2/ graphene nanosheets/ carbon nanotubes composites with high rate capability for supercapacitor applications," *Electrochimica Acta*, 174, 345–355, 2015.

[68] C. Xiang, M. Li, M. Zhi, A. Manivannan, and N. Wu, "A reduced graphene oxide/Co_3O_4 composite for supercapacitor electrode," *Journal of Power Sources*, 226, 65–70, 2013.

[69] Z. J. Han, S. Pineda, A. T. Murdock, D. H. Seo, K. K. Ostrikov, and A. Benda vid, "RuO_2-coated vertical graphene hybrid electrodes for high-performance solid-state supercapacitors," *Journal of Materials Chemistry A*, 5, (33), 17293 17301, 2017.

[70] A. AlaghmandfardandK.Ghandi,"Acomprehensivereviewofgraphiticcar bon nitride (g-C_3N_4)–metal oxide-based nanocomposites: potential for photocatalysis and sensing," *Nanomaterials*, 12, (2), 294, 2022.

[71] E. Ameh, "A review of basic crystallography and x-ray diffraction applica tions," *The international journal of advanced manufacturing technology*, 105, (7), 3289–3302, 2019.

[72] B. E. Warren, X-ray Diffraction. Courier Corporation, 1990.

[73] E. Zolotoyabko, Basic concepts of X-ray diffraction. John Wiley & Sons, 2014.

[74] J. Clay, "The nature of cosmic rays," *Proceedings of the Royal Society of London. Series A-Mathematical and Physical Sciences*, 151, (872), 202–210, 1935.

[75] J. Epp, "X-ray diffraction (xrd) techniques for materials characterization," in

Materials characterization using nondestructive evaluation (NDE) methods, 81–124, *Elsevier*, 2016.

[76] A. A. Bunaciu, E. G. Udriștioiu, and H. Y. Aboul-Enein, "X-ray diffraction: instrumentation and applications," *Critical reviews in analytical chemistry*, 45, (4), 289–299, 2015.

[77] V. Pop, I. Chicinaș, and N. Jumate, Fizica materialelor: metode experimentale. Presa Universitară Clujeană, 2001.

[78] https://database.iem.ac.ru/s-carta.php?ZINCITE+5364. Accesat: 03.2026.

[79] R. Kužel, and S. Daniš, "Structural databases of inorganic materials," *Materials Structure*, 14, (2), 1, 2007.

[80] D. Toloman, A. Gungor, A. Popa, M. Stefan, S. Macavei, L. Barbu-Tudoran, A. Varadi, I. D. Yildirim, R. Suciu, I. Nesterovschi, et al., "Morphological impact on the supercapacitive performance of nanostructured ZnO electrodes," *Ceramics International*, 51, (1), 353–365, 2025.

[81] I. I. Ekanem, A. E. Ikpe, and V. E. Udoh, "Principles of crystal structures for bravais lattice: A study on symmetry within lattice and diffraction lines in crystallography," *Biocompounds*, 1, (1), 1–23, 2024.

[82] I. Chicinas¸, Materiale nanocristaline obtinute prin mecanosinteza. PhD thesis, Fa culty of Physics, Babes-Bolyai University, Cluj-Napoca, Romania, 2005.

[83] A. K. Tripathy, L. Hockaday, J. Clout, and J. Eksteen, "The preparation and characterisation of hydroxycancrinite-type zeolite from the effluent produced from the hydrometallurgical upgrade of iron ore," *Results in Engineering*, 109044, 2026.

[84] B. Hidayat, N. U. W. Sebayang, J. Jamilah, and A. Mahardika, "Brunauer emmett-teller, fourier-transform infrared, and scanning-electron-microscope analysis of biochar from marine organic waste," *SAINS TANAH-Journal of Soil Science and Agroclimatology*, 22, (1), 127–134.

[85] https://www.rruff.net/odr/rruff/sample/odr/view/641212/2010/eyJkd F9pZCI6NzM4LCI3MDY5IjoiUjA1MDQxOSIsInNvcnRfYnki Olt7InNvcn RfZGZfaWQiOiI3MDY5Iiwic29ydF9 kaXIiOiJhc2MifV19. Accesat: 03.2026.

[86] A. C. Sparavigna et al., "Raman broad scans of rare earth oxide (reo) glasses from rruff database, compared to the raman spectra of re oxides from raman open database," *International Journal of Sciences*, 13, (07), 52–64, 2024.

[87] G. Verma and M. Mishra, "Development and optimization of uv-vis spectroscopy-a review," *World Journal of Pharmaceutical Research*, 7, (11), 1170–1180, 2018.

[88] T. H. Gfroerer et al., "Photoluminescence in analysis of surfaces and interfa ces," *Encyclopedia of analytical chemistry*, 67, 3810, 2000.

[89] L. S. Vlasenko, "Point defects in ZnO: Electron paramagnetic resonance study," *Physica B: Condensed Matter*, 404, (23-24), 4774–4778, 2009.

[90] S. Evans, N. Giles, L. Halliburton, and L. Kappers, "Further characterization of oxygen vacancies and zinc vacancies in electron-irradiated ZnO," *Journal of Applied Physics*, 103, (4), 2008.

[91] S. Parashar, B. Murty, S. Repp, S. Weber, and E. Erdem, "Investigation of in trinsic defects in core-shell structured ZnO nanocrystals," *Journal of Applied Physics*, 111, (11), 113712, 2012.

[92] H. Kaftelen, K. Ocakoglu, R. Thomann, S. Tu, S. Weber, and E. Erdem, "EPR and photoluminescence spectroscopy studies on the defect structure of ZnO nanocrystals," *Physical Review B—Condensed Matter and Materials Physics*, 86, (1), 014113, 2012.

[93] S. Wang, J. Zhang, O. Gharbi, V. Vivier, M. Gao, and M. E. Orazem, "Electrochemical impedance spectroscopy," *Nature Reviews Methods Primers*, 1, (1), 41, 2021.

[94] P. T. Kissinger and W. R. Heineman, "Cyclic voltammetry," *Journal of chemical education*, 60, (9), 702, 1983.

[95] F. Marken, A. Neudeck, and A. M. Bond, "Cyclic voltammetry," *Electroanaly tical methods: guide to experiments and applications*, 57–106, 2010.

[96] S. Chevion, M. A. Roberts, and M. Chevion, "The use of cyclic voltammetry for the evaluation of antioxidant capacity," *Free radical biology and medicine*, 28, (6), 860–870, 2000.

[97] P. Chooto and P. Chooto, "Cyclic voltammetry and its applications," *Voltammetry*. IntechOpen, 1, 2019.

[98] J.-M. Saveant, "Molecular catalysis of electrochemical reactions. cyclic voltam metry of systems approaching reversibility," *ACS Catalysis*, 8, (8), 7608–7611, 2018.

[99] P. Ghasemiahangarani, G. Farhan, D. del Mundo, and T. Schoetz, "Charge storage mechanisms in batteries and capacitors: a perspective of the electro-

chemical interface," *Advanced Energy Materials*, 15, (12), 2404704, 2025.

[100] T. Pajkossy and R. Jurczakowski, "Electrochemical impedance spectroscopy in interfacial studies," Current Opinion in *Electrochemistry*, 1, (1), 53–58, 2017.

[101] B.-Y. Chang and S.-M. Park, "Electrochemical impedance spectroscopy," *Annual Review of Analytical Chemistry*, 3, (1), 207–229, 2010.

[102] B.-A. Mei, O. Munteshari, J. Lau, B. Dunn, and L. Pilon, "Physical interpretations of nyquist plots for edlc electrodes and devices," *The Journal of Physical Chemistry C*, 122, (1), 194–206, 2018.

[103] A. Fernandez, E. P´erigo, and R. Faria, "Simulation of galvanostatic charge discharge curves of carbon-based symmetrical electrochemical supercapacitor with organic electrolyte employing potential dependent capacitance and time domain analytical expressions," *Journal of Energy Storage*, 51, 104471, 2022.

[104] M.Z.Iqbal, M.M.Faisal, M.Sulman,S.R.Ali, A.M.Afzal, M.A.Kamran,and T. Alharbi, "Capacitive and diffusive contribution in strontium phosphide polyaniline based supercapattery," *Journal of Energy Storage*, 29, 101324, 2020.

[105] D. Sharma, J. Rajput, B. Kaith, M. Kaur, and S. Sharma, "Synthesis of ZnO nanoparticles and study of their antibacterial and antifungal properties," *Thin solid films*, 519, (3), 1224–1229, 2010.

[106] K. Kairyte, A. Kadys, and Z. Luksiene, "Antibacterial and antifungal activity of photoactivated ZnO nanoparticles in suspension," *Journal of Photochemistry and Photobiology B: Biology*, 128, 78–84, 2013.

[107] N. Bhalla, N. Ingle, A. Jayaprakash, H. Patel, S. V. Patri, and D. Haranath, "Green approach to synthesize nano zinc oxide via moringa oleifera leaves for enhanced anti-oxidant, anti-acne and anti-bacterial properties for health & wellness applications," *Arabian Journal of Chemistry*, 16, (3), 104506, 2023.

[108] X. Huang, X. Zheng, Z. Xu, and C. Yi, "ZnO-based nanocarriers for drug de livery application: From passive to smart strategies," *International journal of pharmaceutics*, 534, (1-2), 190–194, 2017.

[109] K. Senthilkumar, O. Senthilkumar, K. Yamauchi, M. Sato, S. Morito, T. Ohba, M. Nakamura, and Y. Fujita, "Preparation of ZnO nanoparticles for bio imaging applications," *Physica status solidi* (b), 246, (4), 885–888, 2009.

[110] Z. Khabir, A. M. Holmes, Y.-J. Lai, L. Liang, A. Deva, M. A. Polikarpov, M. S. Roberts, and A. V. Zvyagin, "Human epidermal zinc concentrations after to pical application of ZnO nanoparticles in sunscreens," *International Journal of*

Molecular Sciences, 22, (22), 12372, 2021.

[111] N. Kiomarsipour, R. S. Razavi, K. Ghani, and M. Kioumarsipour, "Evaluation of shape and size effects on optical properties of ZnO pigment," *Applied Surface Science*, 270, 33–38, 2013.

[112] P. V. Gayathri, M. P. Rayaroth, C. Aravindakumar, D. Pillai, and S. Joseph, "Sunlight-induced decontamination of water from emerging pharmaceutical pollutants using ZnO nanoparticles," *Chemosphere*, 343, 140265, 2023.

[113] N. Moussa, F. Ebrahim, K. Adly, and M. Hassaan, "Chromium doped ZnO nanoparticles for energy storage, gas and humidity sensing and spin based electronic devices applications," *Optical and Quantum Electronics*, 54, (11), 683, 2022.

[114] K. K. Wong, A. Ng, X. Y. Chen, Y. H. Ng, Y. H. Leung, K. H. Ho, A. B. Djurisic, A. M. C. Ng, W. K. Chan, L. Yu, et al., "Effect of ZnO nanoparticle properties on dye-sensitized solar cell performance," *ACS Applied Materials & Interfaces*, 4, (3), 1254–1261, 2012.

[115] J. E. Eixenberger, C. B. Anders, K. Wada, K. M. Reddy, R. J. Brown, J. Moreno Ramirez, A. E. Weltner, C. Karthik, D. A. Tenne, D. Fologea, et al., "Defect engineering of ZnO nanoparticles for bioimaging applications," *ACS applied materials & interfaces*, 11, (28), 24933–24944, 2019.

[116] R. Hong, T. Pan, J. Qian, and H. Li, "Synthesis and surface modification of ZnOnanoparticles," *Chemical Engineering Journal*, 119, (2-3), 71–81, 2006.

[117] T. Xia, Y. Wang, C. Mai, G. Pan, L. Zhang, W. Zhao, and J. Zhang, "Facile in situ growth of ZnO nanosheets standing on Ni foam as binder-free anodes for lithium ion batteries," *RSC advances*, 9, (34), 19253–19260, 2019.

[118] L. Huang, X. Wang, F. Yin, Y. Zhang, J. Gao, J. Liu, G. Zhou, and Z. Bakenov, "ZnO nanorods grown directly on copper foil substrate as a binder-free anode for high performance lithium-ion batteries," *International Journal of Electroche mical Science*, 11, (10), 8439–8446, 2016.

[119] H.-S. Kim, H. Seo, K. Kim, J. Lee, and J.-H. Kim, "Facile synthesis and elec trochemical properties of carbon-coated ZnO nanotubes for high-rate lithium storage," *Ceramics international*, 44, (15), 18222–18226, 2018.

[120] X. He, J. E. Yoo, M. H. Lee, and J. Bae, "Morphology engineering of ZnO na nostructures for high performance supercapacitors: enhanced electrochemis try of ZnO nanocones compared to ZnO nanowires," *Nanotechnology*, 28, (24),

245402, 2017.

[121] Q. Abbas, M. S. Javed, A. Ahmad, S. H. Siyal, I. Asim, R. Luque, M. D. Alba qami, and A. M. Tighezza, "ZnO nano-flowers assembled on carbon fiber tex tile for high-performance supercapacitor's electrode," *Coatings*, 11, (11), 1337, 2021.

[122] S. Nadupalli, S. Repp, S. Weber, and E. Erdem, "About defect phenomena in ZnOnanocrystals," *Nanoscale*, 13, (20), 9160–9171, 2021.

[123] L. Vlasenko and G. Watkins, "Optical detection of electron paramagnetic resonance for intrinsic defects produced in ZnO by 2.5-mev electron irradiation in situ at 4.2 k," *Physical Review B—Condensed Matter and Materials Physic*s, 72, (3), 035203, 2005.

[124] S. Kasap, I. I. Kaya, S. Repp, and E. Erdem, "Superbat: battery-like supercapa citor utilized by graphene foam and zinc oxide (ZnO) electrodes induced by structural defects," *Nanoscale Advances*, 1, (7), 2586–2597, 2019.

[125] S. Najib, F. Bakan, N. Abdullayeva, R. Bahariqushchi, S. Kasap, G. Franz'o, M.Sankir, N. D. Sankir, S. Mirabella, and E. Erdem, "Tailoring morphology to control defect structures in ZnO electrodes for high-performance supercapacitor devices," *Nanoscale*, 12, (30), 16162–16172, 2020.

[126] A. Janotti and C. G. Van deWalle, "Oxygen vacancies in ZnO," *Applied Physics Letters*, 87, (12), 2005.

[127] D. Jishiashvili, Z. Shiolashvili, E. Sanaia, N. Makhatadze, and A. Jishiash vili, "Morphological changes in zno nano-and microstructures synthesized by pyrolytic technology," in Materials Science Forum, 1166, 71–81, *Trans Tech Publications*, 2025.

[128] S. Vennila, C. Leelavathi, V. Balaprakash, K. Thangavel, S. A. Kumar, J. K. Sundar, and R. Ramesh, "Plant mediated-green synthesis of ZnO nanoparticles as a high capacitance electrode for supercapacitor applications," *Journal of Materials Science: Materials in Electronics*, 36, (8), 489, 2025.

[129] N. A. Mala, A. Singh, S. Bashir, A. Ghosh, A. Padder, S. Arya, N. Thakur, L. Guganathan, R. N. Ali, et al., "Improved electrochemical and photocatalytic performance of the surfactant assisted zinc oxide nanoparticles for supercapacitor and wastewater treatment applications," *Inorganic Chemistry Communications*, 174, 113969, 2025.

[130] P. P. Das, S. Samanta, L. Wang, J. Kim, T. Vogt, P. S. Devi, and Y. Lee, "Redistri

bution of native defects and photoconductivity in ZnO under pressure," *RSC advances*, 9, (8), 4303–4313, 2019.

[131] S. Mustapha, M. Ndamitso, A. Abdulkareem, J. Tijani, D. Shuaib, A. Moham med, and A. Sumaila, "Comparative study of crystallite size using williamson-hall and debye-scherrer plots for ZnO nanoparticles," *Advances in Natural Sciences: Nanoscience and Nanotechnology*, 10, (4), 045013, 2019.

[132] A. Dolgonos, T. O. Mason, and K. R. Poeppelmeier, "Direct optical band gap measurement in polycrystalline semiconductors: A critical look at the tauc method," *Journal of solid state chemistry*, 240, 43–48, 2016.

[133] F. Chen, Y. Chi, H. Zhang, F. Ma, and F. Qin, "Band-gap shrinked NiO@Co3O4 nanotubes as high-performance supercapacitor electrodes," *Journal of Alloys and Compounds*, 888, 161463, 2021.

[134] R. Senger and K. Bajaj, "Optical properties of confined polaronic excitons in spherical ionic quantum dots," *Physical Review B*, 68, (4), 045313, 2003.

[135] K. Davis, R. Yarbrough, M. Froeschle, J. White, and H. Rathnayake, "Band gap engineered zinc oxide nanostructures via a sol–gel synthesis of solvent driven shape-controlled crystal growth," *RSC advances*, 9, (26), 14638–14648, 2019.

[136] J. Wang, R. Chen, Y. Xia, G. Wang, H. Zhao, L. Xiang, and S. Komarneni, "Cost-effective large-scale synthesis of oxygen-defective ZnO photocatalyst with superior activities under uv and visible light," *Ceramics International*, 43, (2), 1870–1879, 2017.

[137] S. Knust, L. Ruhm, A. Kuhlmann, D. Meinderink,J.Buurger, J. K. Lindner, M. T. de los Arcos de Pedro, and G. Grundmeier, "In situ backside raman spectroscopy of zinc oxide nanorods in an atmospheric-pressure dielectric barrier discharge plasma," *Journal of Raman Spectroscopy*, 52, (7), 1237–1245, 2021.

[138] C. Kumari, A.Pandey, andA.Dixit, "Zn interstitial defects and their contribution as efficient light blue emitters in Zn rich ZnO thin films," *Journal of Alloys and Compounds*, 735, 2318–2323, 2018.

[139] F. Oba, M. Choi, A. Togo, and I. Tanaka, "Point defects in ZnO: an approach from first principles," *Science and Technology of Advanced Materials*, 12, (3), 034302, 2011.

[140] D. Fischer, D. Zagorac, and J. C. Schon, "Fundamental insight into the forma tion of the zinc oxide crystal structure," *Thin Solid Films*, 782, 140017, 2023.

[141] H. Fukushima, T. Kozu, H. Shima, H. Funakubo, H. Uchida, T. Katoda, and K. Nishida, "Evaluation of oxygen vacancy in ZnO using raman spectroscopy," in 2015 Joint IEEE International Symposium on the Applications of Ferroelectric (ISAF), International Symposium on Integrated Functionalities (ISIF), and Piezoelectric Force Microscopy Workshop (PFM), 28–31, IEEE, 2015.

[142] S. S. Kanakkillam, B. Krishnan, S. S. Guzman, J. A. A. Martinez, D. A. Ave llaneda, and S. Shaji, "Defects rich nanostructured black zinc oxide formed by nanosecond pulsed laser irradiation in liquid," *Applied Surface Science*, 567, 150858, 2021.

[143] J. Thyr, L. Österlund, and T. Edvinsson, "Polarized and non-polarized raman spectroscopy ofZnOcrystals: Method for determination of crystal growth and crystal plane orientation for nanomaterials," *Journal of Raman Spectroscopy*, 52, (8), 1395–1405, 2021.

[144] W. Feng, P. Huang, B. Wang, C. Wang, W. Wang, T. Wang, S. Chen, R. Lv, Y. Qin, and J. Ma, "Solvothermal synthesis of ZnO with different morphologies in dimethylacetamide media," *Ceramics International*, 42, (2), 2250–2256, 2016.

[145] Y. Song, S. Zhang, C. Zhang, Y. Yang, and K. Lv, "Raman spectra and microstructure of zinc oxide irradiated with swift heavy ion," *Crystals*, 9, (8), 395, 2019.

[146] L. K. Jangir, Y. Kumari, A. Kumar, M. Kumar, and K. Awasthi, "Investigation of luminescence and structural properties of ZnO nanoparticles, synthesized with different precursors," *Materials Chemistry Frontiers*, 1, (7), 1413–1421, 2017.

[147] H. Zeng, G. Duan, Y. Li, S. Yang, X. Xu, and W. Cai, "Blue luminescence of ZnO nanoparticles based on non-equilibrium processes: defect origins and emission controls," *Advanced functional materials*, 20, (4), 561–572, 2010.

[148] B. Debnath, G. Halder, and S. Bhattacharyya, "One-step synthesis, structural and optical characterization of self-assembled ZnO nanoparticle clusters with quench-induced defects," *Science of Advanced Materials*, 6, (6), 1160–1169, 2014.

[149] Y. Gong, T. Andelman, G. F. Neumark, S. O'Brien, and I. L. Kuskovsky, "Ori gin of defect-related green emission from ZnO nanoparticles: effect of surface modification," *Nanoscale Research Letters*, 2, 297–302, 2007.

[150] A. Djurisic, Y. Leung, K. Tam, L. Ding, W. Ge, H. Chen, and S. Gwo, "Green, yellow, and orange defect emission from ZnO nanostructures: Influence of excitation wavelength," *Applied Physics Letters*, 88, (10), 103107, 2006.

[151] A. U. Ammar, I. D. Yildirim, M. H. Aleinawi, M. Buldu-Akturk, N. S. Turhan, S. Nadupalli, A. M. Rostas, and E. Erdem, "Multifrequency EPR spectroscopy study of Mn, Fe, and Cu doped nanocrystalline ZnO," *Materials Research Bulletin*, 160, 112117, 2023.

[152] E. Erdem, "Microwave power, temperature, atmospheric and light dependence of intrinsic defects in ZnO nanoparticles: A study of electron paramagnetic resonance (epr) spectroscopy," *Journal of alloys and compounds*, 605, 34–44, 2014.

[153] E. Erdem, "Defect induced p-type conductivity in zinc oxide at high temperature: Electron paramagnetic resonance spectroscopy," *Nanoscale*, 9, (31), 10983–10986, 2017.

[154] P. Jakes and E. Erdem, "Finite size effects in ZnO nanoparticles: An electron paramagnetic resonance (epr) analysis," *Physica status solidi (RRL)–Rapid Research Letters*, 5, (2), 56–58, 2011.

[155] S. Stoll and A. Schweiger, "Easyspin, a comprehensive software package for spectral simulation and analysis in EPR," *Journal of magnetic resonance*, 178, (1), 42–55, 2006.

[156] J. Wang andH.Zeng,"Recentadvancesinelectrochemical techniques for cha racterizing surface properties of minerals," *Advances in Colloid and Interface Science*, 288, 102346, 2021.

[157] A. M. Afzal, N. Muzaffar, M. W. Iqbal, G. Dastgeer, A. Manzoor, M. Razaq, S. M. Wabaidur, E. A. Al-Ammar, and S. M. Eldin, "Exploring the charge storage mechanism in high-performance Co@MnO_2-based hybrid supercapaci tors using Randles–Ševčík and Dunn's models," *Journal of Applied Electrochemistry*, 54, (1), 65–76, 2024.

[158] K. Pradeeswari, A. Venkatesan, P. Pandi, K. Karthik, K. H. Krishna, and R. M. Kumar, "Studyontheelectrochemical performance of ZnO nanoparticles synthesized via non-aqueous sol-gel route for supercapacitor applications," *Materials Research Express*, 6, (10), 105525, 2019.

[159] A. Eftekhari and M. Mohamedi, "Tailoring pseudocapacitive materials from a mechanistic perspective," *Materials today energy*, 6, 211–229, 2017.

[160] W. Qian, J. Zhu, Y. Zhang, X. Wu, and F. Yan, "Condiment-derived 3d architecture porous carbon for electrochemical supercapacitors," *Small*, 11, (37), 4959–4969, 2015.

[161] X. Du, P. Guo, H. Song, and X. Chen, "Graphene nanosheets as electrode material for electric double-layer capacitors," *Electrochimica Acta*, 55, (16), 4812 4819, 2010.

[162] D. Wang, G. Fang, T. Xue, J. Ma, and G. Geng, "A melt route for the synthesis of activated carbon derived from carton box for high performance symmetric supercapacitor applications," *Journal of Power Sources*, 307, 401–409, 2016.

[163] H. Li, J. Wang, Q. Chu, Z. Wang, F. Zhang, and S. Wang, "Theoretical and experimental specific capacitance of polyaniline in sulfuric acid," *Journal of Power Sources*, 190, (2), 578–586, 2009.

[164] G.Wittstock, M.Burchardt, S. E.Pust, Y. Shen, andC.Zhao, "Scanningelectro chemical microscopy for direct imaging of reaction rates," *Angewandte Chemie International Edition*, 46, (10), 1584–1617, 2007.

[165] J. M. Soon and K. P. Loh, "Electrochemical double-layer capacitance of MoS_2 nanowall films," *Electrochemical and Solid-State Letters*, 10, (11), A250, 2007.

[166] Q. Cao, Z.Shao, D.K.Hensley, N.V.Lavrik, and B.J. Venton, "Influence of geometry on thin layer and diffusion processes at carbon electrodes," Langmuir, 37, (8), 2667–2676, 2021.

[167] J. Chen, W. Li, D. Wang, S. Yang, J. Wen, and Z. Ren, "Electrochemical characterization of carbon nanotubes as electrode in electrochemical double-layer capacitors," *Carbon*, 40, (8), 1193–1197, 2002.

[168] A. Güngör, F. Bakan-Misirlioglu, R. G. Alturk, and E. Erdem, "Elevating su perpacitor performance: Enhancing electrochemical efficiency with transition metal-doped polyaniline electrode," *Journal of Energy Storage*, 76, 110143, 2024.

[169] K. Darowicki, "Differential analysis of impedance data," *Electrochimica acta*, 43, (16-17), 2281–2285, 1998.

[170] J. R. Macdonald and W. B. Johnson, "Fundamentals of impedance spectro scopy," *Impedance spectroscopy: theory, experiment, and applications*, 1–20, 2018.

[171] G. Zeng, Y. Wang, X. Lou, H. Chen, S. Jiang, and W. Zhou, "Vanadium oxide/carbonized chestnut needle composites as cathodematerials for advanced aqueous zinc-ion batteries," *Journal of Energy Storage*, 77, 109859, 2024.

[172] M. Mirzaeian, Q. Abbas, A. Ogwu, P. Hall, M. Goldin, M. Mirzaeian, and H. F. Jirandehi, "Electrode and electrolyte materials for electrochemical capacitors," *International journal of hydrogen energy*, 42, (40), 25565–25587, 2017.

[173] Y. Liu, K. Xiang, W. Zhou, W. Deng, H. Zhu, and H. Chen, "Investigations on tunnel-structure MnO_2 for utilization as a high-voltage and long-life cathode material in aqueousammonium-ionandhybrid-ionbatteries," *Small*, 2308741, 2023.

[174] M. Salanne, B. Rotenberg, K. Naoi, K. Kaneko, P.-L. Taberna, C. P. Grey, B. Dunn, and P. Simon, "Efficient storage mechanisms for building better supercapacitors," *Nature Energy*, 1, (6), 1–10, 2016.

[175] S. G. Avsar, S. Repp, L. Dietel, A. Güngör, S. Weber, K. Ocakoglu, S. Nadupa lli, and E. Erdem, "Competition between charge transfer and energy transfer: Influence of intrinsic defects in ZnO nanocrystals on rhodamine-b dye color signals," *Physical Review B*, 108, (24), L241401, 2023.

[176] K. Kaczmarska, "Esr bottleneck effect in diluted (Gd–Y)Cu_2Si_2 system," *Journal of magnetism and magnetic materials*, 140, 911–912, 1995.

[177] R. Rakhmatullin, V. Semashko, S. Korableva, A. Kiiamov, A. A. Rodionov, R. Tschaggelar, J. A. van Bokhoven, and C. Paun, "EPR study of ceria nano particles containing different concentration of Ce^{3+} ions," *Materials Chemistry and Physics*, 219, 251–257, 2018.

[178] A. Shengelaya, G.-m. Zhao, H. Keller, K. M¨ uller, and B. Kochelaev, "EPR in La1–xCaxMnO_3: Relaxation and bottleneck," *Physical Review B*, 61, (9), 5888, 2000.

[179] C. T. Altaf, T. O. Colak, A. M. Rostas, M. Mihet, M. D. Lazar, I. Iatsunskyi, E. Coy, I. D. Yildirim, F. B. Misirlioglu, E. Erdem, et al., "GO/ZnO-based all solid-state photo-supercapacitors: Effect of GO:ZnO ratio on composite properties and device performance," *Journal of Energy Storage*, 68, 107694, 2023.

[180] D. Malavekar, V. Magdum, S. Khot, J. Kim, and C. Lokhande, "Doping of rare earth elements: Towards enhancing the electrochemical performance of pseudocapacitive materials," *Journal of Alloys and Compounds*, 170601, 2023.

[181] P. Asen, S. Shahrokhian, and A. I. Zad, "Transition metal ions-doped polya niline/graphene oxide nanostructure as high performance electrode for su percapacitor applications," *Journal of Solid State Electrochemistry*, 22, 983–996, 2018.

[182] F. Ali, N. R. Khalid, G. Nabi, A. Ul-Hamid, and M. Ikram, "Hydrothermal synthesis of cerium-doped Co_3O_4 nanoflakes as electrode for supercapacitor application," *International Journal of Energy Research*, 45, (2), 1999–2010, 2021.

[183] S. R. Gawali, D. P. Dubal, V. G. Deonikar, S. S. Patil, S. D. Patil, P. Gomez Romero, D.R.Patil, and J. Pant, "Asymmetric supercapacitor based on nanos tructured ce-doped NiO (Ce: NiO) as positive and reduced graphene oxide (rGO) as negative electrode," *Chemistry Select*, 1, (13), 3471–3478, 2016.

[184] J. Sahu, S. Kumar, F. Ahmed, P. Alvi, B. Dalela, D. Phase, M. Gupta, and S. Da lela, "Electrochemical and electronic structure properties of high-performance supercapacitor based on Nd-doped ZnO nanoparticles," *Journal of Energy Storage*, 59, 106499, 2023.

[185] M. Priyanka, Y. Vidya, H. Manjunatha, G. S. Reddy, T. R. K. Reddy, R. Muni rathnam, E. Krishnakanth, M. Shivanna, and S. Kumar, "Synthesis of yttrium doped zinc oxide nanorods for display, forensic and supercapacitor applications," *Inorganic Chemistry Communications*, 158, 111555, 2023.

[186] M. Karthikeyan, S. Rajkumar, and M. Priyadharshan, "Green synthesis of Ce doped ZnO nanoparticles using phyllanthus emblica seed extract for the efficient high-performance supercapacitor application," *Journal of Industrial and Engineering Chemistry*, 147, 608–618, 2025.

[187] T. K. Pathak, E. Coetsee-Hugo, H.Swart, C.Swart, andR.Kroon, "Preparation and characterization of Ce doped ZnO nanomaterial for photocatalytic and biological applications," *Materials Science and Engineering: B*, 261, 114780, 2020.

[188] A. Mesaros, D. Toloman, M. Nasui, R. Mos, T. Petrisor, B. Vasile, V. Surdu, I. Perhaita, A. Biris, and O. Pana, "A valence states approach for luminescence enhancement by low dopant concentration in Eu-doped ZnO nanoparticles," *Journal of materials science*, 50, 6075–6086, 2015.

[189] R. Kumar, A. Umar, G. Kumar, M. Akhtar, Y. Wang, and S. Kim, "Ce-doped ZnO nanoparticles for efficient photocatalytic degradation of direct red-23 dye," *Ceramics International*, 41, (6), 7773–7782, 2015.

[190] K. Saw, N. Aznan, F. Yam, S. Ng, and S. Pung, "New insights on the Burstein-Moss shift and band gap narrowing in indium-doped zinc oxide thin films," *PloS one*, 10, (10), e0141180, 2015.

[191] A. T. T. Pham, O. K. T. Le, D. Van Hoang, T. H. Nguyen, K.-H. Chen, S. Park, T. B. Phan, and V. C. Tran, "Coupling modification of fermi level, band flattening and lattice defects to approach outstanding thermoelectric performance of ZnO films via tuning In and Ga incorporation," *Acta Materialia*, 241, 118415, 2022.

[192] N. Radutoiu and C. Teodorescu, "Satellites in Ce 3d x-ray photoelectron spectroscopy of ceria.," *Digest Journal of Nanomaterials & Biostructures (DJNB)*, 8, (4), 1535–1549, 2013.

[193] B. Choudhury and A. Choudhury, "Ce^{3+} and oxygen vacancy mediated tuning of structural and optical properties of CeO_2 nanoparticles," *Materials Che mistry and Physics*, 131, (3), 666–671, 2012.

[194] P. Dutta, S. Pal, M. Seehra, Y. Shi, E. Eyring, and R. Ernst, "Concentration of Ce^{3+} and oxygen vacancies in cerium oxide nanoparticles," *Chemistry of Materials*, 18, (21), 5144–5146, 2006.

[195] S. Yuk, D. W. Lee, K.-Y. Song, S. Choi, D.-H. Lee, G. Doo, J. Hyun, J. Kwen, J. Y. Kim, and H.-T. Kim, "Detrimental effect of Ce^{4+} ion on the Pt/c catalyst in polymer electrolyte membrane fuel cells," *Journal of Power Sources*, 448, 227447, 2020.

[196] Y. G. Zhang, G. B. Zhang, and Y. Xu Wang, "First-principles study of the electronic structure and optical properties of Ce-doped ZnO," *Journal of Applied Physics*, 109, (6), 2011.

[197] S. Deshpande, S. Patil, S. V. Kuchibhatla, and S. Seal, "Size dependency varia tion in lattice parameter and valency states in nanocrystalline cerium oxide," *Applied Physics Letters*, 87, (13), 133113, 2005.

[198] M. N. Siddique, A. Ahmed, S. Riyajuddin, M. Faizan, K. Ghosh, and P. Tri pathi, "Exploring the Ce^{3+} ions doping effect on optical and magnetic properties of NiO nanostructures," *Journal of magnetism and magnetic materials*, 500, 166323, 2020.

[199] L. Pidol, O. Guillot-No¨el, A. Kahn-Harari, B. Viana, D. Pelenc, and D. Gourier, "EPR study of Ce^{3+} ions in lutetium silicate scintillators $Lu_2Si_2O_7$ and Lu_2SiO_5," *Journal of Physics and Chemistry of Solids*, 67, (4), 643–650, 2006.

[200] M. Figaj and K. Becker, "An electron paramagnetic resonance study of impurities in ceria, CeO_2," *Solid State Ionics*, 141, 507–512, 2001.

[201] A. Abragam and B. Bleaney, Electron paramagnetic resonance of transition ions. *OUP Oxford*, 2012.

[202] L. Arda, "The effects of Tb doped ZnO nanorod: An EPR study," *Journal of Magnetism and Magnetic Materials*, 475, 493–501, 2019.

[203] M.Cabrera-Baez, E. Padrón-Hernández, J. M. Soares, F. Santos, Y. Guerra, and R. Peña-Garcia, "Effect of yttrium substitution in Fe-doped ZnO nanopar-

ticles: An EPR study," *Journal of Magnetism and Magnetic Materials*, 538, 168317, 2021.

[204] F. Quaranta, A. Valentini, F. R. Rizzi, and G. Casamassima, "Dual-ion-beam sputter deposition of ZnO films," *Journal of Applied Physics*, 74, (1), 244–248, 1993.

[205] B. Guo, Z. Qiu, and K. Wong, "Intensity dependence and transient dynamics of donor–acceptor pair recombination in ZnO thin films grown on (001) sili con," *Applied physics letters*, 82, (14), 2290–2292, 2003.

[206] C.H. Ahn,Y.Y. Kim,D.C. Kim,S.K. Mohanta,and H.K.Cho,"A comparative analysis of deep level emission in ZnO layers deposited by various methods," *Journal of Applied Physics*, 105, (1), 013502, 2009.

[207] B. Cao, W. Cai, and H. Zeng, "Temperature-dependent shifts of three emission bands for ZnO nanoneedle arrays," *Applied physics letters*, 88, (16), 161101, 2006.

[208] N. Shakti, C. Devi, A. Patra, P. Gupta, and S. Kumar, "Lithium doping and photoluminescence properties of ZnO nanorods," *AIP Advances*, 8, (1), 015306, 2018.

[209] C. Abed,C. Bouzidi,H. Elhouichet, B. Gelloz, and M. Ferid, "Mg doping induced high structural quality of sol–gel ZnO nanocrystals: Application in photocatalysis," *Applied Surface Science*, 349, 855–863, 2015.

[210] G. He, H. Fan, L. Ma, K. Wang, C. Liu, D. Ding, and L. Chen, "Dumbbell like ZnO nanoparticles-CeO_2 nanorods composite by one-pot hydrothermal route and their electrochemical charge storage," *Applied Surface Science*, 366, 129–138, 2016.

[211] W. Liu, C. Lu, H. Li, R. Y. Tay, L. Sun, X. Wang, W. L. Chow, X. Wang, B. K. Tay, Z. Chen, et al., "Paper-based all-solid-state flexible micro-supercapacitors with ultra-high rate and rapid frequency response capabilities," *Journal of materials chemistry A*, 4, (10), 3754–3764, 2016.

[212] R. S. Nicholson, "Theory and application of cyclic voltammetry for measurement of electrode reaction kinetics.," *Analytical chemistry*, 37, (11), 1351–1355, 1965.

[213] T. Schoetz, L. Gordon, S. Ivanov, A. Bund, D. Mandler, and R. Messinger, "Disentangling faradaic, pseudocapacitive, and capacitive charge storage: a tutorial for the characterization of batteries, supercapacitors, and hybrid sys-

tems," *Electrochimica Acta*, 412, 140072, 2022.

[214] M. Y. Perdana, B. A. Johan, M. Abdallah, M. E. Hossain, M. A. Aziz, T. N. Baroud, and Q. A. Drmosh, "Understanding the behavior of supercapacitor materials via electrochemical impedance- spectroscopy: A review," *The Chemi cal Record*, e202400007, 2024.

[215] V. Vivier and M.E.Orazem,"Impedance analysis of electrochemical systems," *Chemical Reviews*, 122, (12), 11131–11168, 2022.

[216] H. Morgan, T. Sun, D. Holmes, S. Gawad, and N. G. Green, "Single cell dielectric spectroscopy," *Journal of Physics D: Applied Physics*, 40, (1), 61, 2006.

[217] J.-M. You, D. Kim, and S. Jeon, "Electrocatalytic reduction of H_2O_2 on thiolate graphene oxide covalently to bonded palladium nanoparticles," *Journal of Nanoscience and Nanotechnology*, 12, (5), 3943–3949, 2012.

[218] R. Ramachandran, W. Xuan, C. Zhao, X. Leng, D. Sun, D. Luo, and F. Wang, "Enhanced electrochemical properties of cerium metal–organic framework based composite electrodes for high-performance supercapacitor application," *RSC advances*, 8, (7), 3462–3469, 2018.

[219] L. Zhao, H. Dai, F. Pei, P. Ming, X. Wei, and J. Zhou, "A comparative study of equivalent circuit models for electro-chemical impedance spectroscopy analysis of proton exchange membrane fuel cells," *Energies*, 15, (1), 386, 2022.

[220] S. Rodrigues, N. Munichandraiah, and A. K. Shukla, "AC impedance and state-of-charge analysis of a sealed lithium-ion rechargeable battery," *Journal of Solid State Electrochemistry*, 3, 397–405, 1999.

[221] W. G. Nunes, A. M. Pascon, B. Freitas, L. G. De Sousa, D. V. Franco, H. Zanin, and L. M. Da Silva, "Electrochemical behavior of symmetric electricaldoublelayer capacitors and pseudocapacitors and identification of transport anomalies in the interconnected ionic and electronic phases using the impedance technique," *Nanomaterials*, 12, (4), 676, 2022.

[222] A. J. Khan, L. Gao, M. Sajjad, S. Khan, A. Mateen, A. Ghaffar, I. A. Malik, X. Liao, and G. Zhao, "Synthesis of heterostructured ZnO-CeO_2 nanocomposite for supercapacitor applications," *Inorganic Chemistry Communications*, 159, 111794, 2024.

[223] A.TornheimandD.C.O'Hanlon,"What do coulombic efficiency and capacity retention truly measure? a deep dive into cyclable lithium inventory, limitation type, and redox side reactions," *Journal of The Electrochemical Society*, 167,

(11), 110520, 2020.

[224] A. Ali, M. Ammar, M. Ali, Z. Yahya, M. Y. Javaid, S. ul Hassan, and T. Ah med, "Mo-doped ZnO nanoflakes on Ni-foam for asymmetric supercapacitor applications," *RSC advances*, 9, (47), 27432–27438, 2019.

[225] A. Mohan, V. Manikandan, S. Devanesan, M. S. AlSalhi, C. Rajeevgandhi, S. Guo, and L. Guganathan, "Nanostructured nickel doped zinc oxide material suitable for magnetic, supercapacitor applications and theoretical investigation," *Chemosphere*, 299, 134366, 2022.

[226] M. Stefan, A. M. Rostas, A. U. Ammar, A. Gungor, E. Saritas, D. Toloman, A. Varadi, S. Macavei, L. Barbu-Tudoran, C. Leostean, et al., "Cerium enhanced supercapacitive properties of zinc oxide nanoflowers," *Energy & Fuels*, 38, (19), 19088–19099, 2024.

[227] M. Saranya, R. Ramachandran, and F. Wang, "Graphene-zinc oxide (g-ZnO) nanocomposite for electrochemical supercapacitor applications," *Journal of Science: Advanced Materials and Devices*, 1, (4), 454–460, 2016.

[228] J. Dong, Y. Zhang, M. I. Hussain, W. Zhou, Y. Chen, and L.-N. Wang, "g-C_3N_4: properties, pore modifications, and photocatalytic applications," *Nanomaterials*, 12, (1), 121, 2021.

[229] S. Khasim, A. Pasha, M. Lakshmi, C. Panneerselvam, M. F. Ullah, A. Darwish, T. A. Hamdalla, S.Alfadhli, and S. Al-Ghamdi, "Synthesis of g-C_3N_4/CuO nanocomposite as a supercapacitor with improved electrochemical performance for energy storage applications," *International Journal of Electrochemical Science*, 17, (8), 220838, 2022.

[230] S. Tamang, S. Rai, R. Bhujel, N. K. Bhattacharyya, B. P. Swain, and J. Biswas, "A concise review on GO, rGO and metal oxide/rGO composites: Fabrica tion and their supercapacitor and catalytic applications," *Journal of Alloys and Compounds*, 947, 169588, 2023.

[231] S. Savarimuthu, M. Selvaraj, and H. Chuang, "Electrochemical performance enhancement of ZnO/g-C_3N_4 nanocomposites using urea and thiourea pre cursors for supercapacitor applications," *Inorganic Chemistry Communications*, 178, (Part 2), 2025.

[232] M. Ghorbani, M. R. Golobostanfard, and H. Abdizadeh, "Flexible free standing sandwich type ZnO/rGO/ZnO electrode for wearable supercapacitor," *Applied Surface Science*, 419, 277–285, 2017.

[233] K.Shahid, W.Muhammad, A.Khan, M.Humayun, N.Shah, A.F.Alanazi, and M. Bououdina, "TiO_2/g-C_3N_4 nanocomposite as a dual-functional platform for photocatalytic and electrochemical applications," *Nanocomposites*, 11, (1), 245–270, 2025.

[234] M. Sayed, B. Zhu, P. Kuang, X. Liu, B. Cheng, A. A. A. Ghamdi, S. Wa geh, L. Zhang, and J. Yu, "EPR investigation on electron transfer of 2d/3d g C_3N_4/ZnO s-scheme heterojunction for enhanced CO_2 photoreduction," *Advanced Sustainable Systems*, 6, (1), 2100264, 2022.

[235] D. Dvoranová, M. Mazúr, I. Papailias, T. Giannakopoulou, C. Trapalis, and V. Brezová, "EPR investigations of g-C_3N_4/TiO_2 nanocomposites," *Catalysts*, 8, (2), 47, 2018.

[236] Z.Ma, F.Ren,X.Ming, Y.Long,and A.A.Volinsky,"Cu-doped ZnO electronic structure and optical properties studied by first-principles calculations and experiments," *Materials*, 12, (1), 196, 2019.

[237] M. Sakkaki and S. M. Arab, "Non-catalytic applications of g-C_3N_4: a brief review," *Synthesis and Sintering*, 2, (4), 176–180, 2022.

[238] T. Suter, V. Brázdová, K. McColl, T. S. Miller, H. Nagashima, E. Salvadori, A. Sella, C. A. Howard, C. W. Kay, F. Corà, et al., "Synthesis, structure and electronic properties of graphitic carbon nitride films," *The Journal of Physical Chemistry C*, 122, (44), 25183–25194, 2018.

[239] D. S. Patrick, A. Govind, P. Bharathi, M. K. Mohan, S. Harish, J. Archana, and M. Navaneethan, "Hierarchical ZnO/g-C_3N_4 nanocomposites for enhanced NO_2 gas sensing applications," *Applied Surface Science*, 609, 155337, 2023.

[240] D. Toloman, A. Popa, M. Stan, M. Stefan, G. Vlad, S. Ulinici, G. Baisan, T. D. Silipas, S. Macavei, C. Leostean, et al., "Visible-light-driven photocatalytic de gradation of different organic pollutants using Cu doped ZnO-mwcnt nano composites," *Journal of Alloys and Compounds*, 866, 159010, 2021.

[241] P. Xia, B. Cheng, J. Jiang, and H. Tang, "Localized -conjugated structure and EPR investigation of g-C_3N_4 photocatalyst," *Applied Surface Science*, 487, 335 342, 2019.

[242] B. Babu, T. Aswani, G. T. Rao, R. J. Stella, B. Jayaraja, and R. Ravikumar, "Room temperature ferromagnetism and optical properties of Cu^{2+} doped ZnO nanopowder by ultrasound assisted solid state reaction technique," *Journal of magnetism and magnetic materials*, 355, 76–80, 2014.

[243] D. R. Lorenz, J. R. Wasson, P. R. Johnson, and D. A. Thornton, "Esr studies of alkylamine complexes of copper (ii) imides: the CuN_{42}- chromophore," *Journal of Inorganic and Nuclear Chemistry*, 37, (11), 2297–2302, 1975.

[244] J. P. A. dos Santos, F. C. Rufino, J. I. Y. Ota, R. C. Fernandes, R. Vicentini, C. J. Pagan, L. M. Da Silva, and H. Zanin, "Best practices for electrochemical characterization of supercapacitors," *Journal of Energy Chemistry*, 80, 265–283, 2023.

[245] W. K. Chee, H. N. Lim, I. Harrison, K. F. Chong, Z. Zainal, C. H. Ng, and N. M. Huang, "Performance of flexible and binderless polypyrrole/graphene oxide/zinc oxide supercapacitor electrode in a symmetrical two-electrode configuration," *Electrochimica Acta*, 157, 88–94, 2015.

[246] N. G. Hörmann K.Reuter,"Thermodynamic cyclic voltammograms: peak positions and shapes," *Journal of Physics: Condensed Matter*, 33, (26), 264004, 2021.

[247] H. Zhu,Y. Li,Y. Song,G.Zhao,W. Wu,S. Zhou,D. Wang,and W. Xiao,"Effects of cyclic voltammetric scan rates, scan time, temperatures and carbon addition on sulphation of Pb disc electrodes in aqueous H_2SO_4," *Materials technology*, 35, (3), 135–140, 2020.

[248] D. A. Bograchev, Y. M. Volfkovich, and S. Martemianov, "Diagnostics of supercapacitors using cyclic voltammetry: Modeling and experimental applications," *Journal of Electroanalytical Chemistry*, 935, 117322, 2023.

[249] M. Alexandreli, C. B. Brocchi, D. M. Soares, W. G. Nunes, B. G. Freitas, F. E. de Oliveira, L. E. C. A. Schiavo, A. C. Peterlevitz, L. M. da Silva, and H. Zanin, "Pseudocapacitive behaviour of iron oxides supported on carbon nanofibers as a composite electrode material for aqueous-based supercapacitors," *Journal of Energy Storage*, 42, 103052, 2021.

[250] W. Pholauyphon, P. Charoen-Amornkitt, T. Suzuki, and S. Tsushima, "Perspectives on accurately analyzing cyclic voltammograms for surface-and diffusion-controlled contributions," *Electrochemistry Communications*, 159, 107-654, 2024.

[251] P. Widiatmoko, N. Nugraha, H. Devianto, I. Nurdin, and T. Prakoso, "Upscaled synthesis of carbon nanotube from palm oil mill effluent using pyrolysis for supercapacitor application," in IOP Conference Series: *Materials Science and Engineering*, 823, 012040, IOP Publishing, 2020.

[252] A. C. Lazanas and M. I. Prodromidis, "Electrochemical impedance spectro-

scopy a tutorial," *ACS measurement science au*, 3, (3), 162–193, 2023.

[253] Y. Gogotsi and R. M. Penner, "Energy storage in nanomaterials–capacitive, pseudocapacitive, or battery-like?," *ACS nano*, 12, (3), 2081–2083, 2018.

[254] I. Shaheen, K. S. Ahmad, C. Zequine, R. K. Gupta, A. G. Thomas, and M. Azad Malik, "Sustainable synthesis of organic framework-derived ZnO nanoparticles for fabrication of supercapacitor electrode," *Environmental Technology*, 43, (4), 605–616, 2022.

[255] A. U. Ammar, M. Stan, A. Popa, D. Toloman, S. Macavei, C. Leostean, A. Cio rita, E. Erdem, and A. M. Rostas, "All-in-one supercapacitor devices based on nanosized Mn^{4+}-doped WO_3," *Journal of Energy Storage*, 72, 108599, 2023.

[256] S. Surender, M. Kavipriyah, and S. Balakumar, "Synergistic effect in g C_3N_4/ CuO nanohybrid structures as efficient electrode material for superca pacitor applications," *Inorganic Chemistry Communications*, 150, 110557, 2023.

[257] S. Ahlawat and S. Lata, "Immaculate composite of g-C_3N_4/TiO_2/polypyrrole as a facile super-capacitive electrode material for energy accumulation," *Materials Research Bulletin*, 165, 112328, 2023.

[258] L. M. Jose, N. S. George, S. A. Kadam, D. Nayana, and A. Aravind, "NiO/-C_3N_4 nanocomposites: Dual-function materials for sunlight responsive pho tocatalysis and symmetric supercapacitors," *Inorganic Chemistry Communications*, 178, 114527, 2025.

[259] A. Kumar, H. Mittal, and M. Khanuja, "Facile synthesis of 2d acid-etched g C_3N_4 nanosheets with 1d ZnO nanorods as a promising electrode material for supercapacitor," *Journal of Energy Storage*, 67, 107496, 2023.

[260] C. Harak, V. Kadam, R. Gavhane, S. Balgude, A. Rakshe, N. Brahmankar, S. Uke, D. Satpute, H. Pawar, and S. Mardikar, "Enhanced supercapacitor per formance of a Cu-Fe_2O_3/g-C_3N_4 composite material: synthesis, characteriza tion, and electrochemical analysis," *RSC advances*, 14, (7), 4917–4929, 2024.

[261] L. G. Ghanem, M. A. Hamza, M. M. Taha, and N. K. Allam, "Symmetric supercapacitor devices based on pristine g-C_3N_4 mesoporous nanosheets with exceptional stability and wide operating voltage window," *Journal of Energy Storage*, 52, 104850, 2022.

[262] A.Varadi, A.Silvestru, A.Popa, D.Toloman,A.Rostas,A.U.Ammar,I.Neste rovschi, M. Mihet, S. Macavei, L. Barbu-Tudoran, et al., "Optimizing the Cu^{2+} ions and carbon-related defect centers ratio in g-C_3N_4-ZnO:Cu nanocomposi-

tes for supercapacitor applications," *Journal of Materials Chemistry C*, 14, 3256–3270, 2026.

Anexa A

Appendix

Articles on which this thesis is based

1. Morphological impact on the supercapacitive performance of nanostructured ZnO electrodes

Dana Toloman, Ahmet Gungor, Adriana Popa, Maria Stefan, Sergiu Macavei, Lucian Barbu-Tudoran, **Ana Varadi**, Ipek Deniz Yildirim, Ramona Suciu, Ion Nesterovschi, Maria Mihet, Emre Erdem, Arpad Mihai Rostas

Review: Ceramics International

Quartile: Q1 in Materials Science
Impact Factor = 5.6

2. Cerium Enhanced Supercapacitive Properties of Zinc Oxide Nanoflowers

Maria Stefan, Arpad Mihai Rostas, Ameen Uddin Ammar, Ahmet Güngör, Eminenur Saritas, Dana Toloman, **Ana Varadi**, Sergiu Macavei, Lucian Barbu-Tudoran, Cristian Leostean, Ovidiu Pana, Angela Kasza, Emre Erdem, Adriana Popa

Review: Energy & Fuels

Quartile: Q1
Impact Factor = 5.3

3. Optimizing the Cu^{2+} ion and carbon-related defect center ratio in g-C_3N_4–ZnO:Cu nanocomposites for supercapacitor applications

Ana Varadi, **Anca Silvestru** Adriana Popa, Dana Toloman, Arpad Mihai Rostas, Ameen Uddin Ammar, Ion Nesterovschi, Maria Mihet, Sergiu Macavei, Lucian Barbu-Tudoran, Cristian Leostean, Maria Stefan

Review: Journal of Materials Chemistry C

Quartile: Q2
Impact Factor = 5.2

Articles not directly related to this thesis

4. Enhancing the supercapacitive properties of SnO2 through W^{5+}/W^{6+} redox pairs

Karlo Maskaric, **Ana Varadi**, Ameen Uddin Ammara, Adriana Popa, Dana Toloman, Sergiu Macavei, Lucian Barbu Tudoran, Cristian Leostean, Emre Erdem, Maria Stefan, Arpad Mihai Rostas

Review: Electrochimica Acta

Quartile: Q1
Impact Factor = 5.6

5. Impact of Vanadium ions on the supercapacitive properties of SnO_2 nanoparticles

Ana Varadi, Ion Nesterovschi, Ameen Uddin Ammar, Dana Toloman, Maria Stefan, Cristian Leostean, Sergiu Macavei, Lucian Barbu Tudoran,Feray Bakan Misirlioglu, Marin Senila, Emre Erdem, Arpad Mihai Rostas, Adriana Popa

Review: Journal of Electroanalytical Chemistry

Quartile: Q1
Impact Factor = 4.1